DOT/FAA/AR-02/68

Office of Aviation Research
Washington, D.C. 20591

Effect of Residual and Intercycle Ice Accretions on Airfoil Performance

May 2002

Final Report

This document is available to the U.S. public through the National Technical Information Service (NTIS), Springfield, Virginia 22161.

U.S. Department of Transportation
Federal Aviation Administration

NOTICE

Technical Report Documentation Page

1. Report No.	2. Government Accession No.	3. Recipient's Catalog No.
DOT/FAA/AR-02/68		

4. Title and Subtitle	5. Report Date
EFFECT OF RESIDUAL AND INTERCYCLE ICE ACCRETIONS ON AIRFOIL PERFORMANCE	May 2002
	6. Performing Organization Code

7. Author(s)	8. Performing Organization Report No.
Andy P. Broeren and Michael B. Bragg	

9. Performing Organization Name and Address	10. Work Unit No. (TRAIS)
University of Illinois at Urbana-Champaign Aeronautical and Astronautical Engineering Urbana, IL 61801	11. Contract or Grant No.

12. Sponsoring Agency Name and Address	13. Type of Report and Period Covered
U.S. Department of Transportation Federal Aviation Administration Office of Aviation Research Washington, DC 20591	Final Report
	14. Sponsoring Agency Code AIR-100

15. Supplementary Notes

The FAA William J. Hughes Technical Center COTR was Mr. James T. Riley.

16. Abstract

This report describes the results of an experimental study designed to characterize and evaluate the aerodynamic performance penalties of residual and intercycle ice accretions that result from the cyclic operation of a typical aircraft deicing system. Icing wind tunnel tests were carried out on a 36-inch chord NACA 23012 airfoil section equipped with a pneumatic deicer for several different cloud conditions modeled after FAR 25 Appendix C. Results from the icing tests showed that the intercycle ice accretions were much more severe in terms of size and shape than the residual ice accretions. Molds of selected intercycle ice shapes were made and converted to castings that were attached to the leading edge of a 36-inch chord NACA 23012 airfoil model for aerodynamic testing. The aerodynamic testing revealed that the intercycle ice shapes caused a significant performance degradation. Maximum lift coefficients were typically reduced about 60% from 1.8 (clean) to 0.7 (iced) and stall angles were reduced from 17 deg. (clean) to 9 deg. (iced). Changes in the Reynolds number (from 2.0×10^6 to 10.5×10^6) and Mach number (from 0.10 to 0.28) did not significantly affect the iced-airfoil performance coefficients.

17. Key Words	18. Distribution Statement
Pneumatic deicer system, Residual ice, Intercycle ice, Performance degradation	This document is available to the public through the National Technical Information Service (NTIS) Springfield, Virginia 22161.

19. Security Classif. (of this report)	20. Security Classif. (of this page)	21. No. of Pages	22. Price
Unclassified	Unclassified	55	

TABLE OF CONTENTS

LIST OF FIGURES

LIST OF TABLES

LIST OF ACRONYMS AND SYMBOLS

$C_{l,\alpha}$	Lift-curve slope
$C_{l,max}$	Maximum lift coefficient
CNC	Computer-numerically controlled
FAA	Federal Aviation Administration
FAR	Federal Aviation Regulation
GRC	Glenn Research Center
k/c	Nondimensional roughness height
LTPT	Low-Turbulence Pressure Tunnel
LaRC	NASA Langley Research Center
LWC	Liquid water content
Ma	Mach number
MVD	Median volumetric diameter
NASA	National Aeronautics and Space Administration
Re	Reynolds number
x/c	Nondimensional chordwise location

EXECUTIVE SUMMARY

This report presents the results of an experimental study designed to evaluate the aerodynamic performance penalties of residual and intercycle ice accretions. Such ice accretions result from the cyclic operation of typical aircraft deicing systems. Residual ice is defined as the ice accretion present on the deicer surface immediately after deicer activation. Intercycle ice is defined as the ice accretion present on the deicer surface immediately before deicer activation. Both of these definitions only apply after the deicer has been activated for several cycles, thereby reaching a steady state of ice accretion and shedding.

The overall objectives of this study were two-fold. The first objective was to characterize the size, shape, roughness, etc. of residual and intercycle ice accretions formed on an airfoil equipped with a pneumatic deicer. The second was to measure the aerodynamic performance penalties of the cast ice accretions and determine if more detailed study was warranted.

Ice accretion testing was carried out on a NACA 23012 airfoil section having a 36-inch chord and equipped with a pneumatic deicer. The icing runs were performed at several different cloud conditions modeled after FAR 25 Appendix C. The Reynolds and Mach numbers were 6.5×10^6 and 0.27, respectively. Residual and intercycle ice shapes were generated at 0° and 4° angle of attack. For selected intercycle shapes, molds were made of the accretions and were later converted into castings for aerodynamic testing. The aerodynamic performance testing was carried out using a similar 36-inch chord NACA 23012 airfoil model. The model had removable leading edges so that four different castings of the intercycle ice shapes could be installed in place of the clean leading edge. Aerodynamic measurements were performed over a Reynolds number range of 3.5×10^6 to 10.5×10^6 and over a Mach number range of 0.12 to 0.28. Tests were also conducted with standard, uniformly distributed roughness in the form of 40- and 80-grit sandpaper applied to the airfoil leading edge.

Results from the ice accretion testing showed that the intercycle ice accretions were much larger in size and surface extent than the residual ice accretions. The size of the intercycle ice accretions was reduced by using 1-minute boot cycles for conditions where 3-minute cycles were originally used. The intercycle ice shapes were found to be independent of when the deicer was initially activated. That is, the deicer was equally effective when activated at the first indication of icing (spray on) versus when activated after a quarter-inch of ice was allowed to accrete. The intercycle ice accretions tended to be fairly repeatable from run-to-run.

Aerodynamic testing revealed that the intercycle ice shapes caused significant performance degradation. Maximum lift values were typically reduced from 1.8 (clean) to 0.7 (iced) and stall angle values were reduced from 17° (clean) to 9° (iced). The minimum drag coefficient increased from 0.007 (clean) to 0.026 (iced). An increase in Reynolds number at a constant Mach number of 0.12 had virtually no effect on the lift curve or the stall. Mach number variation at constant Reynolds number had a small effect, decreasing the maximum lift with increasing Mach number. The 40- and 80-grit sandpaper was not adequate in simulating the intercycle ice shape performance degradation. Maximum lift values were typically reduced from 1.8 (clean) to 1.2 (sandpapered) and stall angles were reduced from 17° (clean) to 12° (sandpapered). The minimum drag coefficient increased from 0.007 (clean) to 0.011 (sandpapered). The sandpaper

roughness was not large enough to accurately simulate even the nominal heights of the intercycle shapes, as it was smaller by nearly a factor of five. Also, the sandpaper did not have the ridge-like features of the actual accretions.

The very large performance degradation associated with the intercycle ice shapes implies that more detailed study may be warranted. A remaining question is what effect scale has on the ice accretion geometry. The 36-inch chord models used in this study were not representative of a typical wing chord. Reasonable questions may arise about how the present data apply to characteristics and resulting performance degradation of ice accretions obtained on a larger scale model. This would primarily affect the ice accretion geometry, since this study has shown that Reynolds and Mach number effects on performance are very small in the iced case. Because intercycle ice accretions and pneumatic boot operation cannot be scaled reliably, the acquisition and testing of full-scale intercycle ice accretions would provide valuable data to confirm the aerodynamic performance degradation observed in this study.

1. INTRODUCTION.

The cyclic operation of typical pneumatic aircraft deicing systems leads to the formation of residual and intercycle ice accretions. For example, pneumatic boots may be inflated and deflated at 1-minute or 3-minute intervals, depending upon the severity of icing. The ice accretion present on the deicer surface just prior to its initial activation is the "preactivation" ice. After the system has been cycled a sufficient number of times, the periodic activation and ice accretion cycle reaches steady state. After steady state has been reached, "intercycle" ice refers to the ice shape as it exists immediately before subsequent activations of the deicer. This is not to be confused with "residual ice" which refers to any ice that remains on the surface immediately after the deicer activation. This report addresses the characteristics of residual and intercycle ice accretions for a given airfoil and deicing system along with the aerodynamic performance penalties of intercycle ice accretions.

1.1 REVIEW OF LITERATURE.

The general effects of ice accretions on airfoil performance are well known—decreased lift and increased drag, and have been researched extensively for several years. Many survey papers exist; for example, Lee, Kim, and Bragg [1] reported on ice shape location, size, geometry, and other effects on airfoil performance. However, the case of intercycle ice is different in that data on the characteristics of the ice shapes themselves are more scarce. Shin and Bond [2] analyzed the characteristics of residual and intercycle ice accretions for pneumatic and several other deicing systems installed on a NACA 0012 airfoil. The reported results were for 1-minute cycling times and showed that the deicers generally cleaned the leading edge, leaving little residual ice. The intercycle ice, therefore, would accrete during the 1-minute periods leading up to the deicer operation. The height (k) of this intercycle ice roughness, normalized by chord (c), varied from approximately $k/c = 0.002$ to 0.010, depending upon the icing condition (i.e., glaze or rime) and the type of deicer. Shin and Bond [2] concluded that the intercycle ice would have an effect on airfoil and wing performance and that uniformly distributed roughness may not be an appropriate simulation of the actual intercycle ice. No aerodynamic measurements were performed during the study.

There are a small number of previous studies in the public domain that included measurements of the aerodynamic performance effects of residual and intercycle ice accretions. Albright, et al. [3] measured the drag coefficient before and after the operation of a pneumatic deicer on a NACA 65_1-215 airfoil. The general results showed that the intercycle ice (before deicer operation) caused a higher drag coefficient than the residual ice (after deicer operation), and that both were higher than for the clean airfoil. Similar research was done by Bowden [4] for a NACA 0011 airfoil. Bowden also showed how the lift coefficient decreased as ice was accreted and then increased when the boot was cycled and the ice shed. The results of these studies were taken from a recent review of residual ice characteristics and performance penalties and the reader is encouraged to consult Reichhold and Bragg [5] for more details. While these reports provided meaningful data on the performance effects of residual and intercycle ice accretions, a major shortcoming was that the data were acquired at fixed angle of attack. Therefore, the change in the airfoil stall characteristics was not documented.

The effect of intercycle ice accretions on airfoil-stalling characteristics was considered as part of a larger study by Jackson and Bragg [6]. Tracings were made of intercycle ice shapes produced on a 4-foot chord NLF-0414 airfoil for one icing cloud condition and for 1-minute cycling times. These tracings were used to produce two-dimensional (i.e., no spanwise variation in cross-section) ice shape simulations that were geometrically scaled and attached to the leading edge of a 1.5-foot chord NLF-0414 airfoil model. While the degradation in maximum lift was on the order of 30%, the tests were conducted on a small scale at low Reynolds number (less than 2.0×10^6). In addition, the effect of the three-dimensional nature of intercycle ice accretions was not quantified.

1.2 BACKGROUND.

The brief literature survey above shows there are valuable studies in the public domain, but more information is needed. Particularly, the effect of residual and intercycle ice accretions formed at one angle of attack on airfoil performance over its operating range is largely unknown. Recently, some questions have been raised concerning the effects of residual and intercycle ice for turbopropeller and piston aircraft employing pneumatic boot deicing systems [7, 8]. Since little relevant data were available, the Federal Aviation Administration (FAA), in collaboration with the National Aeronautics and Space Administration (NASA), initiated a study to assess the potential aerodynamic severity of residual and intercycle ice accretions. This effort also involved researchers at the University of Illinois and BFGoodrich (now known as Goodrich) Aerospace De-icing and Specialty Systems Division, with participation by some aircraft manufacturers.

Riley, et al. [9] described the scope of this work in a recent conference paper and some of the salient points are repeated here. This research program is intended to produce information that is both representative and applicable to aircraft that use pneumatic boots. Therefore, the experiments were designed to study ice accretions that could be regarded as forming on a generic system representative of those used in the turbopropeller and piston aircraft industry. This research program is not focused on the performance of an ice protection system on any particular aircraft currently in use.

1.3 RESEARCH OBJECTIVES AND OVERVIEW.

The overall objectives of this study were two-fold: (1) to characterize the size, shape, roughness, etc. of residual and intercycle ice accretions formed on an airfoil equipped with a pneumatic deicer and (2) to measure the aerodynamic performance penalties of the cast ice accretions and determine if more detailed study is warranted.

A NACA 23012 airfoil was selected for this study since it is representative of wing airfoil sections used on aircraft currently in operation. The airfoil model had a 36-inch chord and was equipped with a pneumatic-deicing boot provided by BFGoodrich. The residual and intercycle ice accretions were generated in the BFGoodrich icing wind tunnel and were molded using procedures developed at the NASA Glenn Research Center (GRC). It should be noted that only intercycle ice accretions were molded because the residual ice roughness was too small to be duplicated using this method.

From these molds, castings were made that attached to the leading edge of another 36-inch chord NACA 23012 airfoil model in the NASA Langley (LaRC) Low-Turbulence Pressure Tunnel (LTPT). Subsequent airfoil performance measurements were made over a large range of angle of attack, Reynolds and Mach numbers. In addition, measurements were performed with 40- and 80-grit paper-backed garnet sandpaper that represented a standard, uniformly distributed roughness.

2. ICE ACCRETION TESTING.

This section presents all aspects of the residual and intercycle ice accretion testing. The facility and model are described first, followed by a discussion of the test matrix and documentation methods, and finally, the key results. More details concerning the ice accretion testing and results can be found in reference [10]10.

2.1 FACILITY AND MODEL.

All of the ice accretion testing was performed in the BFGoodrich icing wind tunnel. This facility is a closed-loop refrigerated wind tunnel equipped with seven heated spray bars containing NASA-type nozzles. The test section dimensions were 22″ wide by 44″ high by 60″ in length. A cold room was adjacent to the test section and was used for ice shape documentation and mold making. The NACA 23012 airfoil model was mounted horizontally in the test section and was supported on each end by 1-inch thick aluminum turning plates. The model had a 36-inch chord and was computer-numerically controlled (CNC) machined aluminum. The leading edge of the model was recessed to accommodate a flush-mounted BFGoodrich pneumatic deicer type 29S having a nominal thickness of 0.085-inch with outer layers of neoprene. The deicer contained five spanwise tubes as shown in figure 1. During the testing, these boots were used in series with a larger set of boots outside of the tunnel. With this system, it was possible to closely simulate the inflation rate of a typical (full-scale) aircraft deicer system. The system timer controlled the pressurized air to inflate both sets of boots simultaneously. A pressure transducer was used to provide continuous monitoring of the inflated pressure—nominally 18 psig. Partial vacuum was used to deflate and hold down the boot tubes. The boot operation was computer-controlled and was set up for 1- or 3-minute cycles.

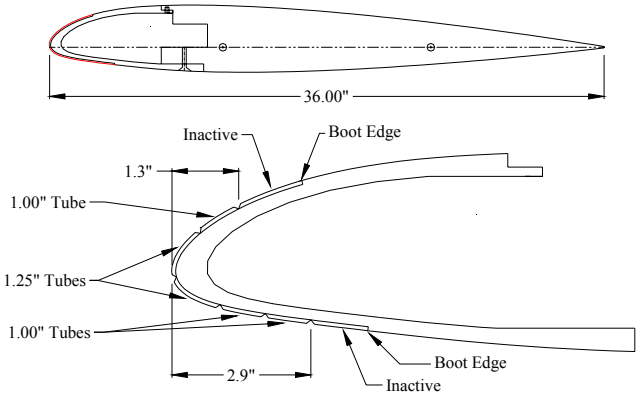

FIGURE 1. SCHEMATIC OF THE NACA 23012 MODEL USED FOR THE ICE ACCRETION TESTING

2.2 TEST MATRIX AND PROCEDURE.

The icing-cloud conditions for this experiment were selected from Federal Aviation Regulation (FAR) 25 Appendix C. These conditions were meant to cover a range of rime, mixed, and glaze icing. The droplet median volumetric diameters (MVDs) were either 20 or 40 μm and the static temperatures were -4°, 14°, and 21°F. (One run was performed at -22°F.) The "continuous maximum" conditions had lower liquid water contents (LWCs) in the range of 0.15 to 0.65 g/m^3, while the "intermittent maximum" conditions had higher LWCs, in the range of 0.25 to 2.20 g/m^3. The airfoil model was tested at either 0° or 4° angle of attack at the maximum tunnel speed of 200 mph. This corresponded to $Re = 6.5\times10^6$ and $Ma = 0.27$, for 14°F. (Note that some high LWC icing cloud conditions limited the maximum tunnel speed; these cases were run at 175 mph.)

The deicing boots were activated shortly after the spray was turned on. The activation time was calculated based upon a simple model of a Rosemount ice detector probe, taking into account the cloud conditions for each run. The activation time varied from 2 to 34 seconds (depending upon conditions) and was based on estimation of the exposure time to icing when the detector would first annunciate. After the boots were first activated, a 12-minute spray time was used for the continuous maximum conditions along with 3-minute boot cycles. A 3-minute spray time was used for the intermittent maximum conditions along with 1-minute boot cycles. The 1- and 3-minute boot cycle intervals were selected as being typical of current automated deicing boot systems. The 3-minute deicing cycle was selected as being typical for icing intensities associated with continuous maximum icing conditions, and the 1-minute deicing cycle was selected as being typical for icing intensities associated with the higher LWC of intermittent maximum icing conditions.

The details of the run conditions are listed in tables 1 through 4. The tables are organized by either continuous maximum conditions (tables 1 and 2) or intermittent maximum conditions (tables 3 and 4) and by angle of attack. The last two columns show how many runs were performed for intercycle or residual ice documentation. As indicated by the tables, more emphasis was placed on the intercycle ice documentation since the amount of ice was larger and more amenable to molding. Repeat runs were performed at several of the conditions to gauge the typical run-to-run variation of the intercycle ice accretions.

TABLE 1. SUMMARY OF RUNS PERFORMED FOR CONTINUOUS MAXIMUM CONDITIONS FOR 0° ANGLE OF ATTACK

Droplet MVD (μm)	Static Temp. (°F)	Droplet LWC (g/m^3)	Activation Time (sec)	No. of Intercycle Ice Runs	No. of Residual Ice Runs
20	-22	0.15	34	1	0
20	-4	0.25	20	1	1
20	14	0.45	11	8	1
20	21	0.65	8	3	1
40	-4	0.25	19	2	1
40	14	0.25	19	1	0
40	21	0.25	19	2	1

TABLE 2. SUMMARY OF RUNS PERFORMED FOR CONTINUOUS MAXIMUM CONDITIONS FOR 4° ANGLE OF ATTACK

Droplet MVD (μm)	Static Temp. (°F)	Droplet LWC (g/m^3)	Activation Time (sec)	No. of Intercycle Ice Runs	No. of Residual Ice Runs
20	-4	0.25	20	3	0
20	14	0.45	11	0	0
20	21	0.65	8	0	0
40	-4	0.25	19	1	0
40	14	0.25	19	3	0
40	21	0.25	19	1	0

TABLE 3. SUMMARY OF RUNS PERFORMED FOR INTERMITTENT MAXIMUM CONDITIONS FOR 0° ANGLE OF ATTACK

Droplet MVD (μm)	Static Temp. (°F)	Droplet LWC (g/m^3)	Activation Time (sec)	No. of Intercycle Ice Runs	No. of Residual Ice Runs
20	-4	1.70	3	1	0
20	14	1.95	3	1	0
20	21	2.20	2	1	0
40	-4	0.40	12	3	1
40	14	0.52	9	1	0
40	21	0.68	7	2	0

TABLE 4. SUMMARY OF RUNS PERFORMED FOR INTERMITTENT MAXIMUM CONDITIONS FOR 4° ANGLE OF ATTACK

Droplet MVD (μm)	Static Temp. (°F)	Droplet LWC (g/m^3)	Activation Time (sec)	No. of Intercycle Ice Runs	No. of Residual Ice Runs
20	-4	1.70	3	0	0
20	14	1.95	3	3	0
20	21	2.20	2	1	0
40	-4	0.40	12	1	0
40	14	0.52	9	1	0
40	21	0.68	7	1	0

The documentation of residual and intercycle shapes was performed during and at the end of each run. During the run, a video camera recorded the ice build-up and shedding as the boots were cycled. The BFGoodrich OPTRON was used to measure the ice thickness near the airfoil leading edge at midspan. At the end of each run, the standard methods of documentation included tracings at three spanwise locations, ice height (or thickness) measurements, and photographs. In the case of the intercycle shapes, the spray was turned off and the last boot cycle was not performed. So there were four boot cycles for the continuous maximum cases (12-minute spray) and three boot cycles for the intermittent maximum cases (3-minute spray). The residual ice shapes were recorded immediately after the last boot cycle with the spray turned off. So for residual ice there were actually five boot cycles for the continuous maximum cases and four boot cycles for the intermittent maximum cases. For selected intercycle ice shapes, molds

were made using a special process developed at NASA GRC. No molds were made of the residual ice cases since there was little ice accretion remaining. Several repeat runs were made of the mold cases to ensure that the ice accretions were representative of that case and not an anomaly. A total of six molds were made of intercycle accretions and the conditions are listed in table 5. The table also indicates the ice shapes that were selected for aerodynamic testing.

TABLE 5. SUMMARY OF INTERCYCLE ICE ACCRETIONS THAT WERE DOCUMENTED WITH MOLDS

Ice Shape	Angle of Attack (deg.)	Droplet MVD (μm)	Static Temp. (°F)	Droplet LWC (g/m^3)	Spray Time (min.)	Boot Cycle (min.)
290*	0	20	14	0.45	12	3
296*	0	20	21	0.65	12	3
302	4	20	-4	0.25	12	3
312*	0	40	21	0.25	12	3
322*	0	40	-4	0.40	3	1
330	4	20	14	1.95	3	1

* Ice shape selected for aerodynamic testing.

2.3 RESULTS.

The overall objective of the ice accretion testing was to characterize the size, shape, roughness, etc., of the residual and intercycle ice accretions. Specific to this objective was the generation of molds from representative accretions that could later be used for aerodynamic testing. In general, the cases selected for molds tended to have larger masses of ice (particularly on the upper surface), thereby representing a "worst-case scenario." As indicated in table 5, this tended to occur more for the continuous maximum cases that had a 3-minute boot cycle and for 0° angle of attack. For these conditions, a significant accretion formed during the 3-minute cycle. On the other hand, the intermittent maximum cases tended to have less ice owing to the 1-minute cycle. This occurred despite the higher water loading associated with the intermittent maximum cases.

These icing effects are illustrated in the figures 2 through 7. Each figure shows a tracing and a photograph corresponding to the mold runs listed in table 5. The photographs are for the actual run that was molded, except for run 290 in figure 2. The photograph in figure 2 is from run 292, which was a repeat of run 290. All of the tracings shown in figures 2 through 7 were taken at the model midspan and were also from repeat runs. The tracings are for repeat runs because if tracings had been taken at midspan for the mold cases, the tracing process would have altered the ice shape that was molded.

The ice shapes selected for aerodynamic testing were from runs 290, 296, 312, and 322. These were chosen because they provided a reasonable variation in cloud conditions and ice shape type. For example, ice shape 290 (cf. figure 2) represents a mixed glaze/rime shape for a continuous maximum case. Ice shapes 296 and 312 (cf. figures 3 and 5) are both glaze type shapes, but the ridge-like features on the upper surface are quite different. This is most likely caused by the difference in droplet MVD. Finally, ice shape 322 (cf. figure 6) represents both rime ice and

intermittent maximum cases. All cases selected were for 0° angle of attack, which tended to have residual and intercycle ice further aft on the upper surface.

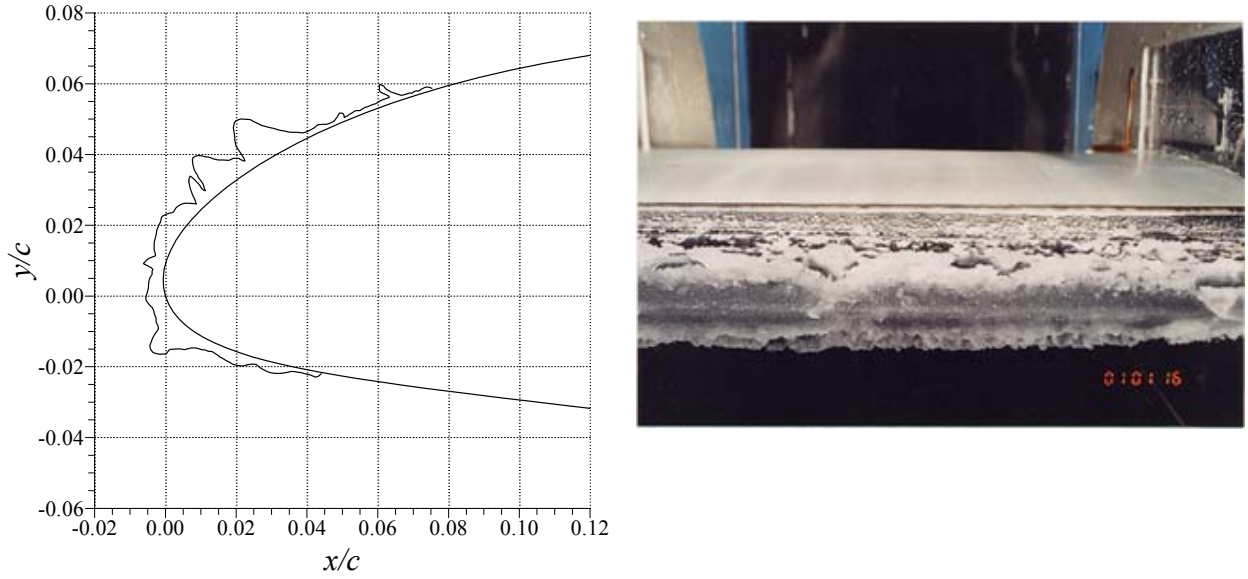

FIGURE 2. ICE ACCRETION CHARACTERISTICS FOR RUN 290, TRACING FROM RUN 288, AND PHOTOGRAPH FROM RUN 292 (REPEAT RUNS)

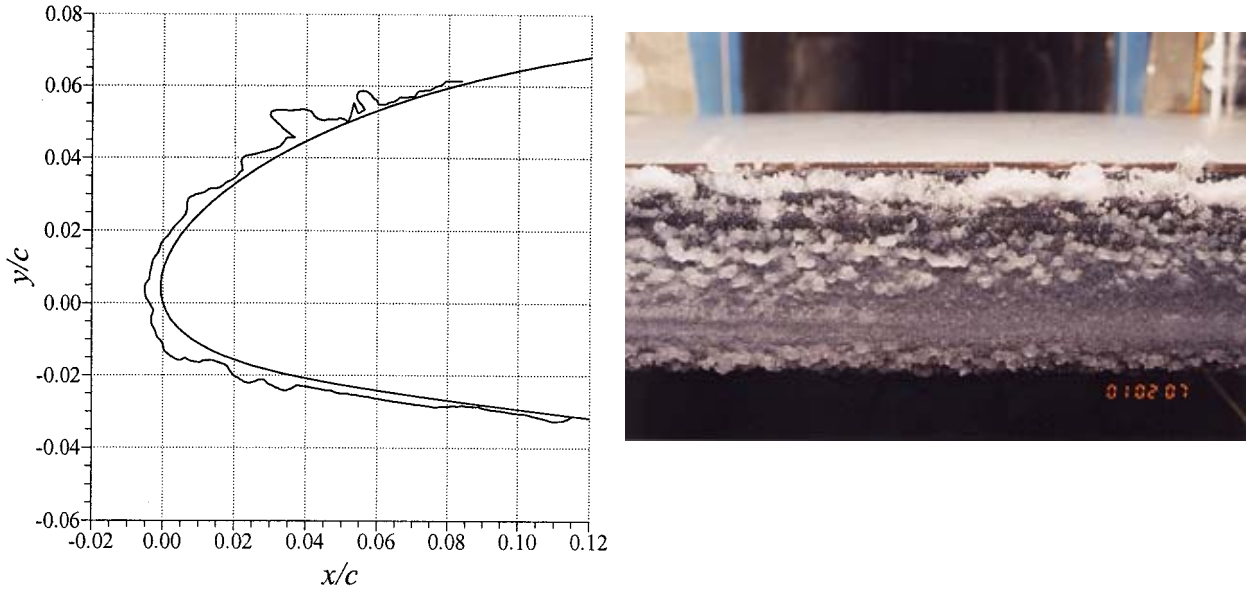

FIGURE 3. ICE ACCRETION CHARACTERISTICS FOR RUN 296, TRACING FROM RUN 293 (REPEAT RUN), AND PHOTOGRAPH FROM RUN 296

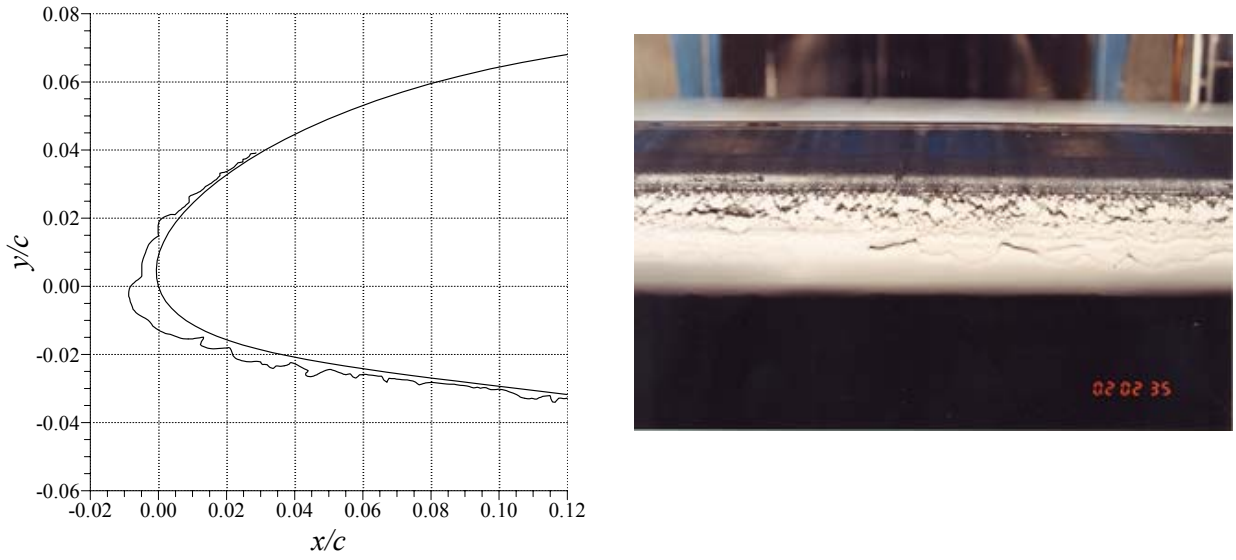

FIGURE 4. ICE ACCRETION CHARACTERISTICS FOR RUN 302, TRACING FROM RUN 301 (REPEAT RUN), AND PHOTOGRAPH FROM RUN 302

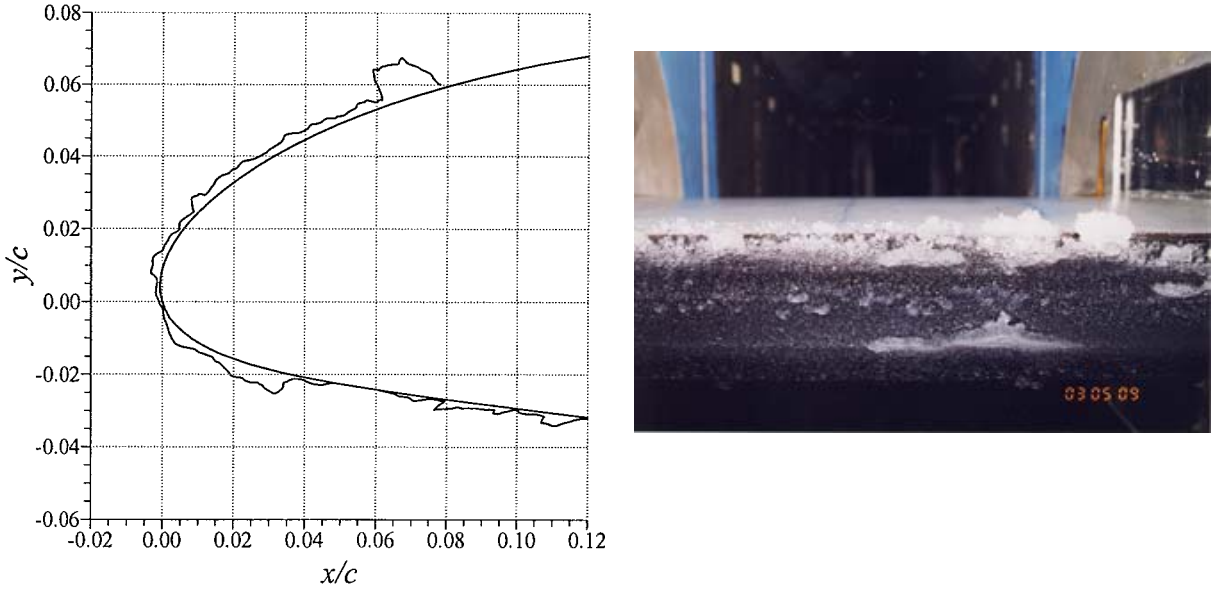

FIGURE 5. ICE ACCRETION CHARACTERISTICS FOR RUN 312, TRACING FROM RUN 310 (REPEAT RUN), AND PHOTOGRAPH FROM RUN 312

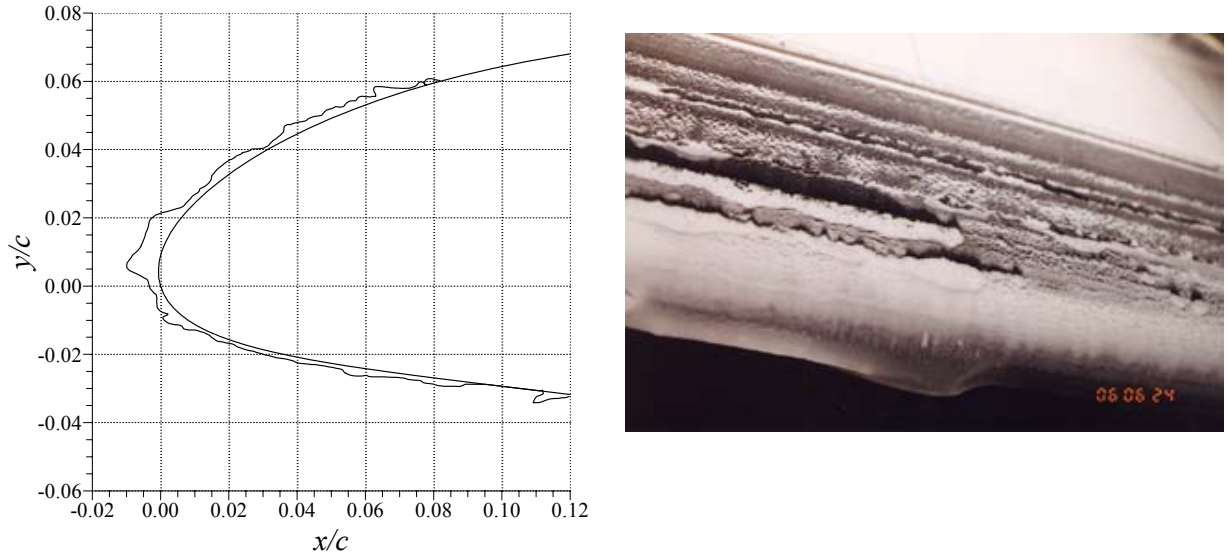

FIGURE 6. ICE ACCRETION CHARACTERISTICS FOR RUN 322, TRACING FROM RUN 320 (REPEAT RUN), AND PHOTOGRAPH FROM RUN 322

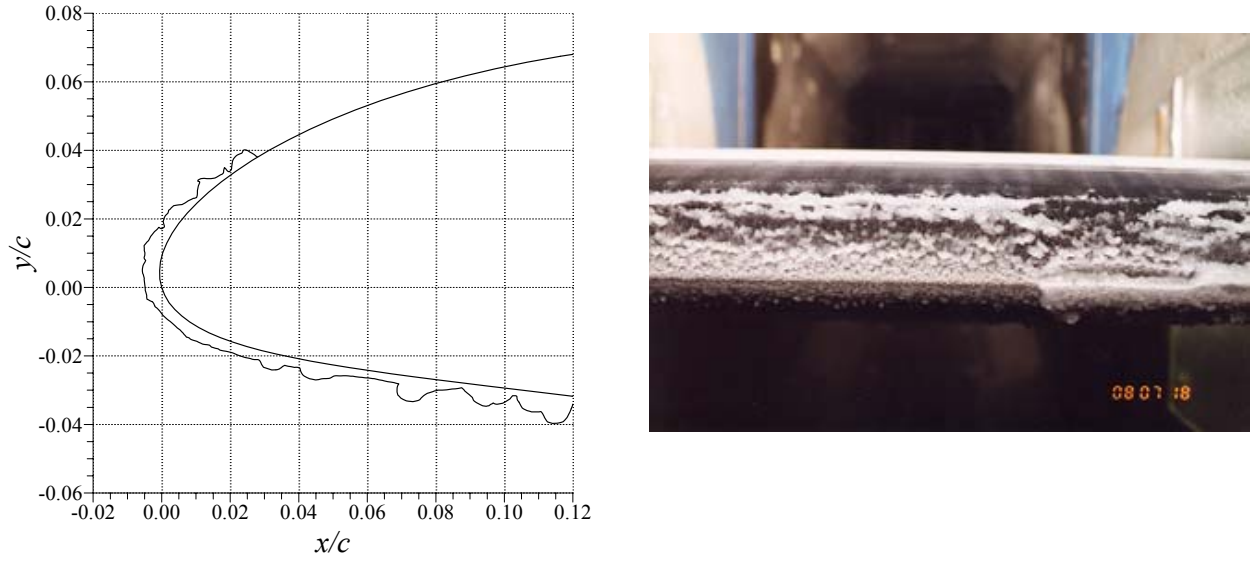

FIGURE 7. ICE ACCRETION CHARACTERISTICS FOR RUN 330, TRACING FROM RUN 329 (REPEAT RUN), AND PHOTOGRAPH FROM RUN 330

Through the course of the ice accretion testing, several observations were made. First, the choice of spray times was adequate to reach steady state. The residual and intercycle ice shapes reached a steady state after two or three boot cycles. Thus, the use of three and four cycles was conservative in this regard. This was also verified by running a case with a 24-minute spray. There was little quantifiable difference between the residual and intercycle ice shapes for this case and those for the usual 12-minute spray.

The amount of residual ice tended to be very small relative to the intercycle shapes. This is illustrated in figure 8 which shows a photograph and tracing of a residual ice case corresponding to the ice shape 290 shown in figure 2. The leading edge of the model in the area of the first two tubes was completely clean and the residual ice that remained was small and not uniform across the span. Since there was a large amount of ice that accreted during the 3-minute cycle, this case was repeated using 1-minute cycles. A 12-minute spray was used and the results are comparable since the ice accretions tend to steady state after two or three cycles. This ice accretion is shown in figure 9. The maximum ice height normalized by chord (k/c) was 0.007. For the 3-minute cycle case shown in figure 2, the maximum heights were approximately 0.014, or double the size. These results imply that a 1-minute cycle time would be more effective than a 3-minute cycle time, at least for the case that was tested.

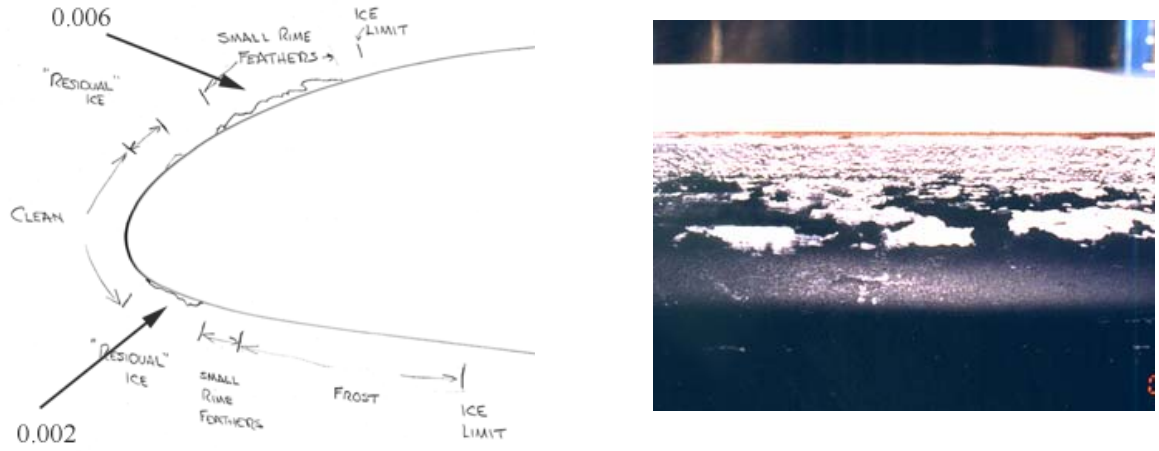

FIGURE 8. TRACING AND PHOTOGRAPH OF RESIDUAL ICE RUN 297. RESIDUAL ICE CORRESPONDS TO INTERCYCLE ICE RUN 290. ROUGHNESS HEIGHTS (0.006, 0.002) NORMALIZED BY CHORD (k/c).

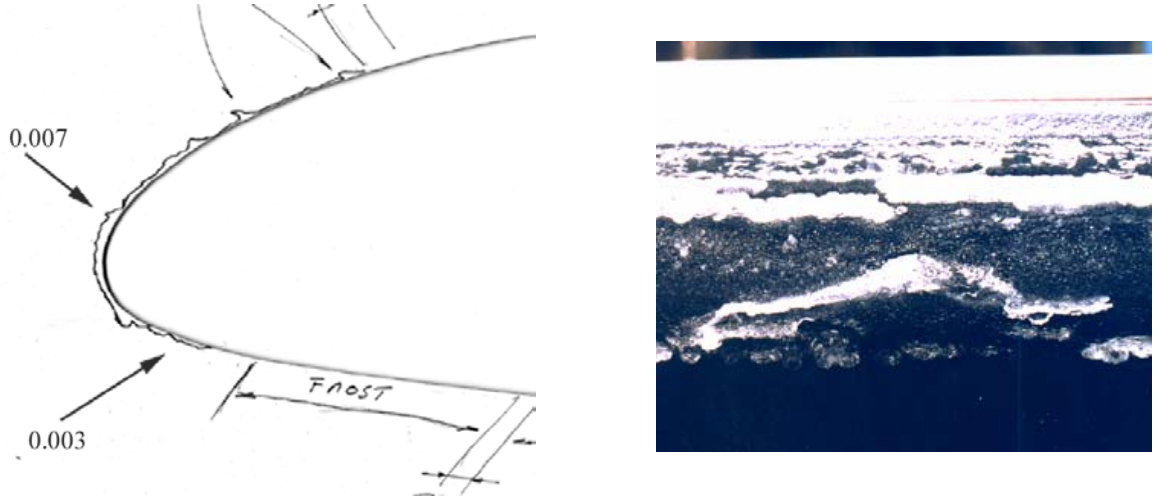

FIGURE 9. TRACING AND PHOTOGRAPH OF INTERCYCLE ICE RUN 326. CLOUD CONDITIONS SAME AS RUN 290, WITH 1-minute BOOT CYCLE. ROUGHNESS HEIGHTS (0.007, 0.003) NORMALIZED BY CHORD (k/c).

Another parameter of interest was the deicer initial activation time. For the cloud conditions associated with ice shape 290 (cf. table 5), the initial activation time was varied over a large range. The usual activation time was 11 seconds after the spray was first turned on. This was based upon the estimated time of ice-detector annunciation as described above. Three other runs were conducted with activation times of 30, 120, and 252 seconds. The 252 seconds corresponded to the amount of time required to accumulate 0.25 inch of ice on the leading edge as measured by the OPTRON ice detector. The results showed virtually no variation in the residual and intercycle ice shapes after two or three boot cycles. For this condition, the final ice shape was independent of the amount of ice present on the airfoil at the initial activation. This implies that turning the system on as soon as ice is detected does not hinder the deicer performance, at least for the case that was tested.

3. AERODYNAMIC TESTING.

This section details the aerodynamic testing carried out at NASA Langley's Low-Turbulence Pressure Tunnel (LTPT). A description of the facility and model is presented first, followed by the test matrix and procedures, and finally the key results. More details concerning the aerodynamic testing and results can be found in reference 10.

3.1 FACILITY AND MODEL.

The NASA Langley LTPT is a closed-return tunnel that can be pressurized so as to independently vary Reynolds and Mach numbers. The LTPT is capable of simulating near-flight Reynolds and Mach numbers for two-dimensional airfoils. For these tests, the free-stream test-section turbulence intensity was 0.1% or less. The inlet contraction ratio was 17.6 to 1 and the rectangular test-section dimensions were 36″ wide by 90″ high. The 36-inch chord NACA 23012 airfoil model was supported horizontally between two large turning plates.

The test section was equipped with a sidewall boundary-layer control system that was used to mitigate three-dimensional effects. This system was originally developed for testing high-lift airfoil configurations, and a description of this system was given by Pascal, et al. [11]. A section of porous plate was imbedded in the turning plates that supported the model. The porous plate was located along the airfoil upper surface from approximately $x/c = 0.35$ running to the trailing edge. It extended approximately 0.75 inches above the airfoil surface. Manifolds were located behind each section of porous plate and were connected to a series of pipes that ran out of the pressurized area.

During tunnel operation, valves in the piping system were adjusted to obtain the desired amount of venting. The system is referred to as a "venting" system since sidewall suction was achieved by venting through the porous plate to atmospheric pressure. This means that the amount of venting (e.g., mass flow) available was a function of the operating pressure. For example, no venting was available with the tunnel running at atmospheric pressure. Most of the data for this study was acquired with sidewall venting. However, some runs were performed with no venting to help gauge its effect. The sidewall venting mass flow rates depended on the tunnel condition (e.g., Mach and Reynolds number) and was determined by the LTPT staff from previous experience. In actual practice, some of the selected mass flow rates were adjusted slightly based

on the spanwise pressure distribution across the airfoil. The venting system was not originally designed nor optimized for this model configuration.

The NACA 23012 airfoil model was CNC machined from solid aluminum and had recessed openings for pressure instrumentation. The model was designed and built with a removable leading edge. There were two leading edges, one used for baseline runs for the clean airfoil and an alternate leading edge used for ice shape runs. Ice shape castings were made from the molds acquired during the icing tests using a special process developed at NASA GRC. The ice shape castings were mounted to the alternate leading edge. This method simulated the actual ice shape with very high fidelity. In addition, an "instrumentation slice" was installed near the model midspan. The instrumentation slice was cut out of stainless steel to match the ice shape cross-section and had pressure taps distributed around the ice shape contour. This allowed for a good approximate measurement of the pressure distribution around the ice shape and provided pressures for determining the lift and pitching-moment coefficients. The baseline model had 67 static pressure orifices along the main chordwise row and 17 orifices in a spanwise row located at $x/c = 0.70$ on the upper surface. The photograph in figure 10 shows the model mounted in the test section, with ice shape and pressure instrumentation slice attached to the airfoil leading edge.

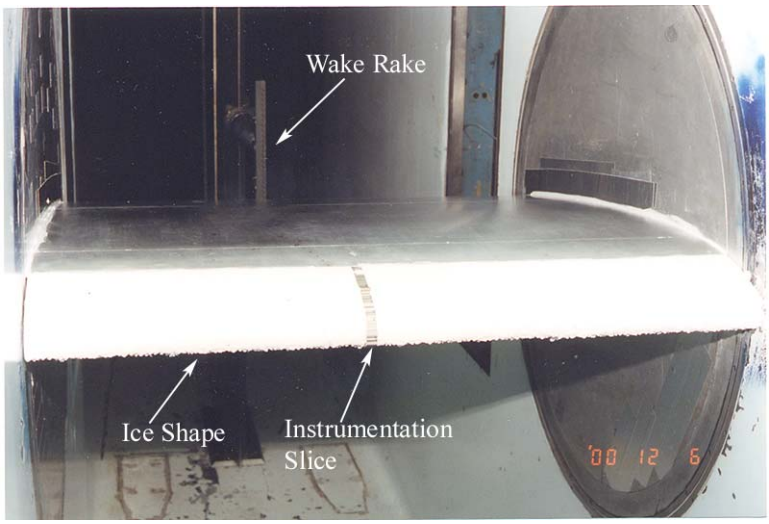

FIGURE 10. PHOTOGRAPH OF NACA 23012 AIRFOIL MODEL WITH ICE SHAPE MOUNTED IN THE LTPT TEST SECTION, VIEW LOOKING DOWNSTREAM

The LTPT was equipped with a three-component force balance; however, it was designed for operation at much higher dynamic pressures than were run in this experiment. Therefore, the data from the balance was deemed unreliable and lift and pitching-moment data were obtained from the integration of surface static pressures. The pitching-moment coefficient reported here was determined for the quarter-chord location. Drag coefficients were calculated from wake pressures measured with a wake rake (i.e., a wake survey) using the standard moment-deficit methods. One-degree angle of attack increments were used for all data collection, except for the wake drag, which was acquired in two-degree increments. Corrections to the integrated performance coefficients accounting for solid and wake blockage and streamline curvature were applied to the data during postprocessing using the methods of Allen and Vincenti [12].

3.2 TEST MATRIX AND PROCEDURE.

The test matrix was selected to yield a broad range of Reynolds and Mach numbers with conditions being applicable to turbopropeller and piston aircraft as constrained by the limitations of the facility. Table 6 summarizes these conditions for the clean, tripped, and iced airfoil configurations. All of these conditions corresponded to stagnation pressures above the atmosphere, from approximately 20 to 60 psia. In addition to this, some runs were also performed at $Re = 2.0\times10^6$ at atmospheric pressure where the Mach number was nominally 0.095. The matrix was designed to isolate the effects of Reynolds and Mach number. Therefore, there is a Reynolds number variation from 3.5×10^6 to 10.5×10^6 at a fixed Mach number of 0.12. Likewise, there is a Mach number variation from 0.12 to 0.28 at constant Reynolds numbers of 7.5×10^6 and 10.5×10^6. The matrix shown in table 6 was run with sidewall venting. A subset of this matrix was run with no sidewall venting for selected configurations.

The test matrix indicates that runs were performed with the boundary layer tripped. This testing was performed to facilitate comparison with data from other experimental facilities or computations. Two trips were applied to the model, one at $x/c = 0.02$ on the upper surface and one at $x/c = 0.05$ on the lower surface. The trips consisted of a very sparse array of 80- to 100-grit glass microbeads (0.0083 to 0.0059 inches in diameter, $k/c = 0.00023$ to 0.00016) on a 0.003-inch-thick substrate of double-backed tape that was 0.25 inches wide. The iced cases refer to both the ice shape castings described above and the standard roughness. The standard roughness was 40- and 80-grit paper-backed garnet sandpaper that covered the leading edge from $x/c = 0.10$ on the upper surface to $x/c = 0.07$ on the lower surface. The overall heights (including the paper substrate) for the 40- and 80-grit sandpapers was 0.044 inch ($k/c = 0.0012$) and 0.022 inch ($k/c = 0.0006$), respectively. Additionally, this was attached to the model surface with 0.003-inch-thick, double-backed tape.

TABLE 6. LTPT AERODYNAMIC PERFORMANCE TEST MATRIX

Reynolds Number	Mach Number		
	0.12	0.21	0.28
3.5×10^6	Clean, Tripped, Iced		
7.5×10^6	Clean, Tripped, Iced	Clean, Iced	Clean, Iced
10.5×10^6	Clean, Tripped, Iced		Clean, Tripped, Iced

3.3 RESULTS.

The LTPT testing was very successful in generating a large amount of valuable data. Since the test matrix was designed to isolate the independent effects of Reynolds and Mach number variations, the data are typically presented so as to depict these effects independently. Since some data were acquired with and some without sidewall venting, it is important to note that all data presented in this report were acquired using sidewall venting, unless otherwise stated. The results showed that sidewall venting had no significant effect on either the clean or iced airfoil data. The minor effects of sidewall venting are addressed in appendix A. The clean airfoil results are discussed first and provide the necessary baseline to gauge the performance degradation of the intercycle ice accretions and sandpaper roughness.

3.3.1 Clean Airfoil Results.

The clean airfoil results are organized in the following way. The effects of Reynolds and Mach number variation on the integrated performance coefficients are presented first (see figures 11-13). The data are then compared to available historical data (see figures 14-17). More analysis of the clean airfoil data is given in appendix B.

Overall, the clean airfoil results followed classic airfoil behavior and compared favorably with historical data. Figure 11 shows the effect of Reynolds number variation at constant Mach number on the performance coefficients. As expected, the maximum lift coefficient ($C_{l,max}$) increased significantly from $Re = 3.5\times10^6$ to $Re = 7.5\times10^6$. This increase in $C_{l,max}$ was approximately 0.1. Predictable results were also observed in the drag data where the drag coefficients tended to decrease with increasing Reynolds number, particularly for higher angles of attack. The effect of Mach number variation at constant Reynolds number is illustrated in figures 12 and 13. Again, classic airfoil behavior was observed in the performance coefficients. The lift-curve slope ($C_{l,\alpha}$) increased with increasing Mach number, but the $C_{l,max}$ decreased about 0.1 from $Ma = 0.12$ to $Ma = 0.28$, for $Re = 10.5\times10^6$ as shown in figure 13. A more noticeable change occurred in the stalling angle of attack (α_{stall}), which decreased about 2 degrees from $Ma = 0.12$ to $Ma = 0.28$ for $Re = 10.5\times10^6$ in figure 13. The data in figure 13 for $Ma = 0.28$ stop at $\alpha = 15.6°$ because the flow became unsteady as the airfoil stalled while the angle of attack was increased. Since this condition corresponded to a high dynamic pressure, the run had to be aborted at this angle of attack for safety reasons. The increasing $C_{l,\alpha}$ (observed in both figures 12 and 13) occurred along with an attendant increase in the drag. The variation in the pitching moment (about quarter-chord) indicates that the airfoil became more front-loaded, at higher angle of attack, as the Mach number increased.

While these Reynolds and Mach number trends illustrate classic behavior, they are also consistent with previous airfoil tests conducted in the LTPT. For example, Ladson [13] analyzed data from the testing of a NACA 0012 airfoil having a 24-inch chord. These data were acquired with solid sidewalls (no sidewall boundary-layer control). The independent effect of Reynolds and Mach numbers on $C_{l,max}$ was nearly identical to the present results. These data illustrate the pitfalls of testing airfoils in atmospheric tunnels where the Reynolds and Mach numbers cannot be independently controlled. For example, one apparent anomaly would be that $C_{l,max}$ and α_{stall} both would appear to decrease with increasing Reynolds number. Another, perhaps more startling anomaly would be increasing drag with increasing Reynolds number.

The independent effects of Reynolds and Mach numbers on the performance coefficients must also be considered when comparing data from different facilities or with historical data. For example, the NACA 23012 data in Abbott and von Doenhoff [14] were for large Reynolds number variations (from 3.0×10^6 to 9.0×10^6), but the Mach number variation was not reported. The authors do say that the Mach numbers were "less than about 0.17." Despite the Mach number vagueness, the Abbott and von Doenhoff data are suitable for comparison to the present data set. Before these plots are discussed, it is worthwhile to note other procedural details about the historical data. Coincidentally, the data were acquired in the LTPT, although perhaps not known by this name at the time. The NACA 23012 model had a 24-inch chord and it is reasonable to assume that no sidewall venting capabilities existed. The lift coefficients were

determined "by integration of pressures representing the reaction on the floor and ceiling of the tunnel." That is, no airfoil surface pressures were available as in the present data. The pitching moment data were "measured directly by a balance." The drag coefficients were determined from wake surveys. The authors do not mention if the data were corrected for solid-boundary effects such as solid and wake blockage.

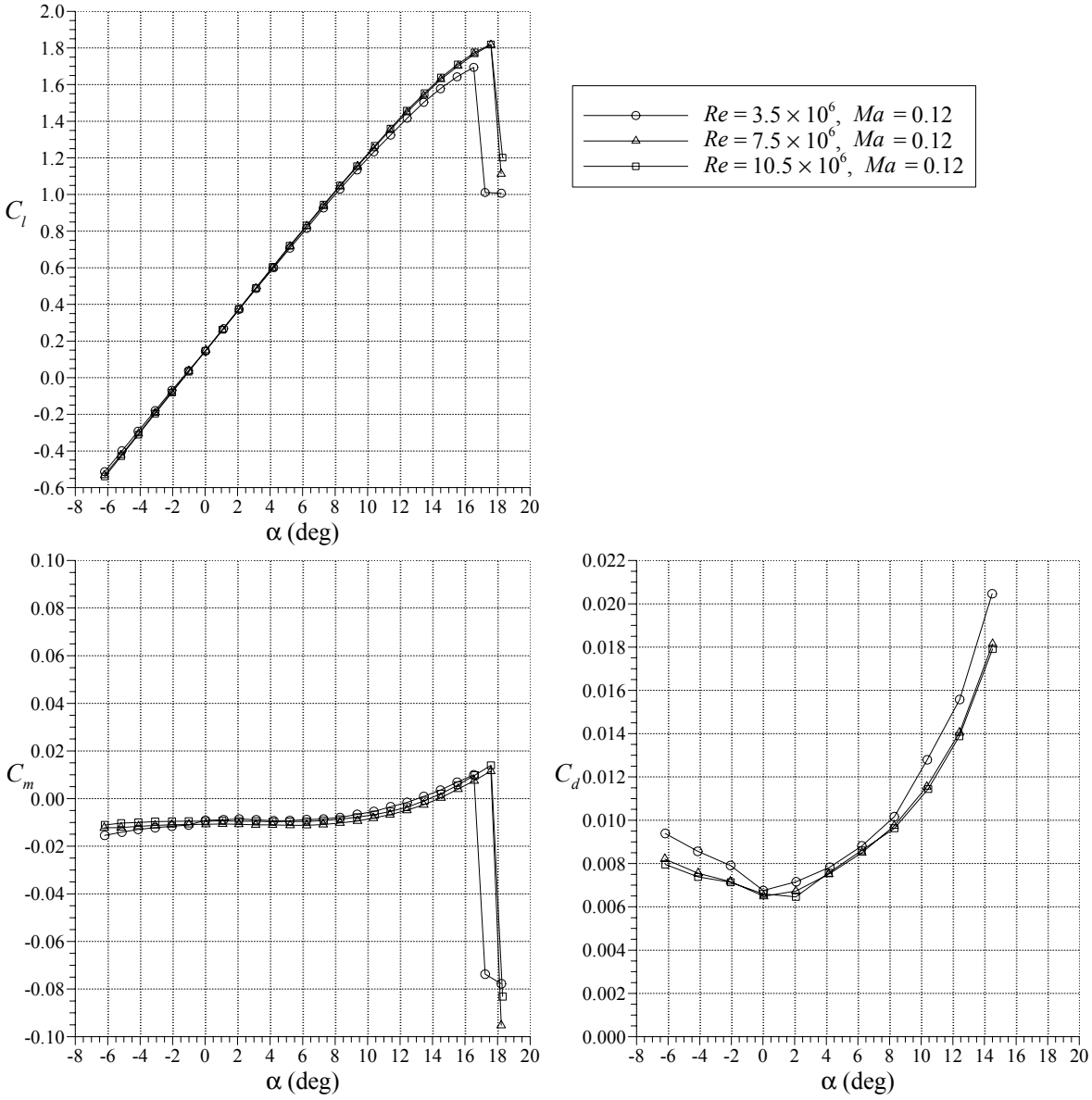

FIGURE 11. EFFECT OF REYNOLDS NUMBER AT CONSTANT MACH NUMBER ON THE PERFORMANCE OF THE CLEAN NACA 23012 AIRFOIL

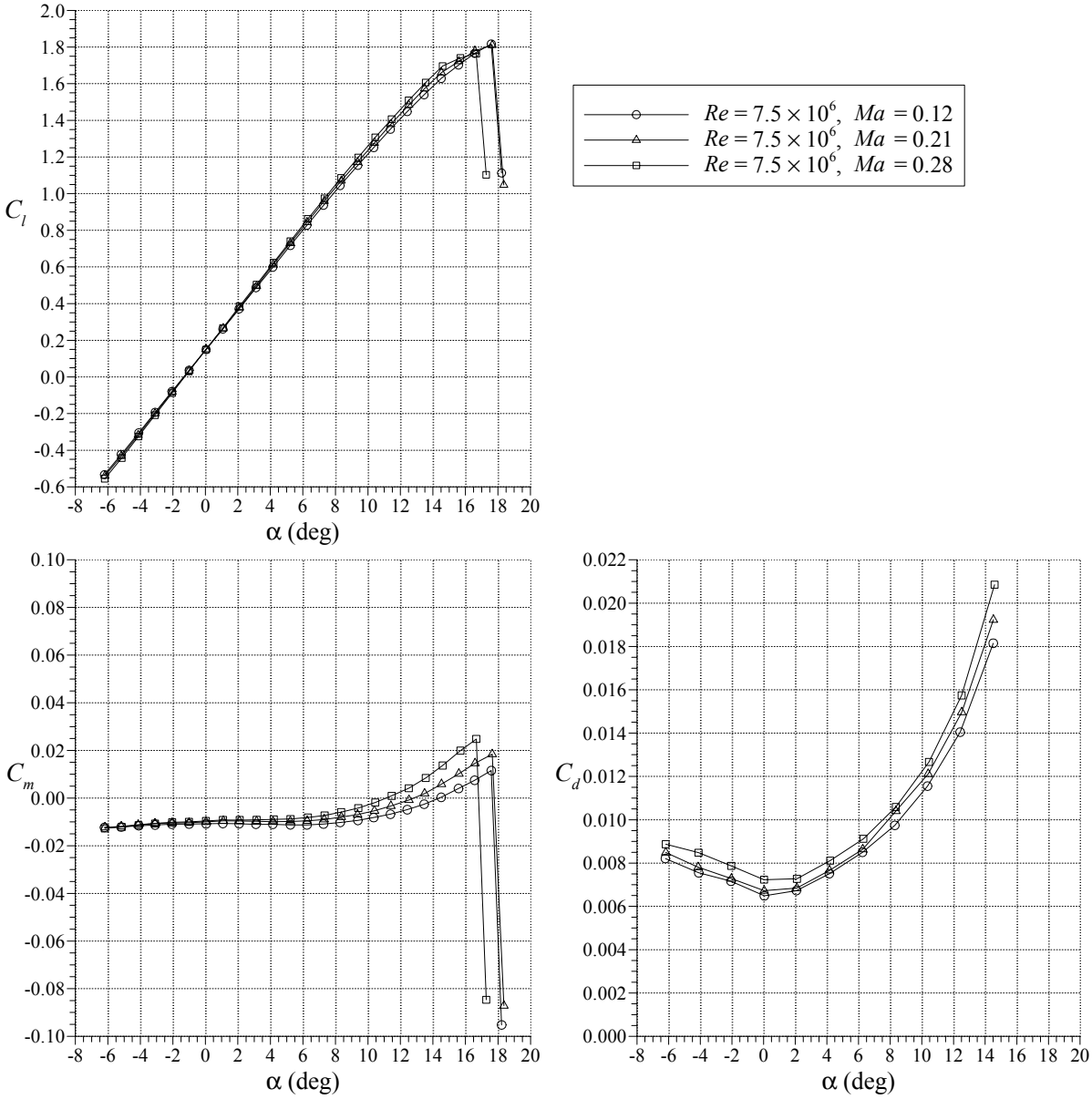

FIGURE 12. EFFECT OF MACH NUMBER AT CONSTANT REYNOLDS NUMBER OF 7.5×10^6 ON THE PERFORMANCE OF THE CLEAN NACA 23012 AIRFOIL

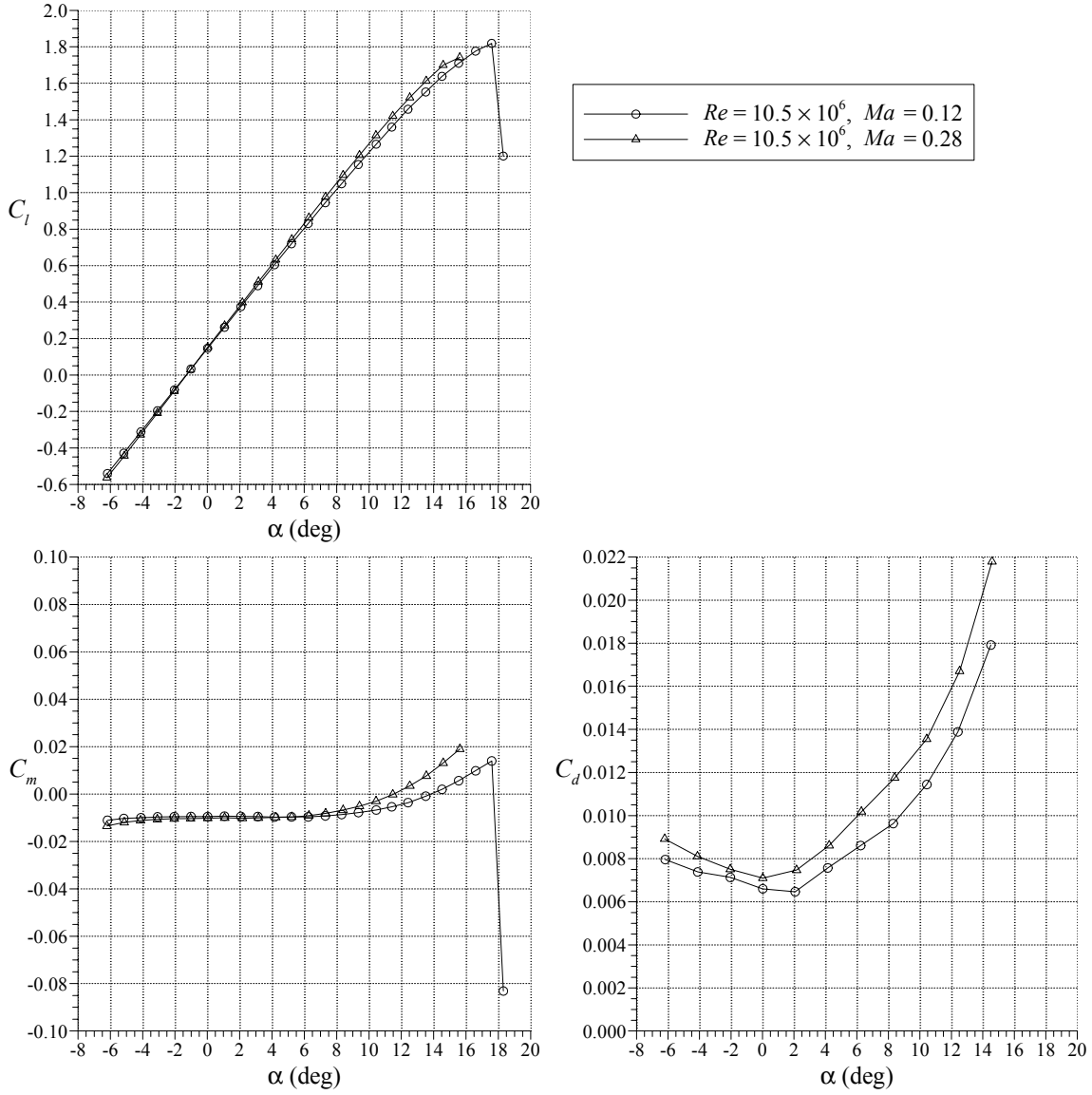

FIGURE 13. EFFECT OF MACH NUMBER AT CONSTANT REYNOLDS NUMBER OF 10.5×10^6 ON THE PERFORMANCE OF THE CLEAN NACA 23012 AIRFOIL

The present data are co-plotted with data extracted from the plots in Abbott and von Doenhoff in figures 14 through 16. Figure 14 shows the present data for $Re = 3.5 \times 10^6$ and $Ma = 0.12$ compared with historical data for $Re = 3.0 \times 10^6$ and $Ma < 0.17$. The plots show that the lift coefficient data from Abbott and von Doenhoff matched the present data very well in the linear range. The difference in pitching moments was likely due to two major factors. First, extracting C_m data from the plots in Abbott and von Doenhoff was difficult because of the poor resolution in the scale divisions. Secondly, no details were given about the balance used to measure the pitching moment. It is reasonable to assume that this balance was designed for the large-pitching moments associated with multi-element airfoils (some of these data are also shown in Abbott and von Doenhoff) operating at the high dynamic pressures available for the facility. Therefore, the

relatively low-pitching moments for the single-element NACA 23012 airfoil may have been difficult to resolve accurately. Finally, the drag coefficients for the historical data were significantly smaller than for the present data. For the present data, it is possible that the presence of the pressure orifices may have caused slightly higher drag values. There was also a spanwise seam located at $x/c = 0.21$ on the upper and lower surface where the removable leading edge joined the main body of the airfoil. It is likely that this may have influenced the boundary layer and resulting drag measurement as well. These data are analyzed in more detail in appendix B.

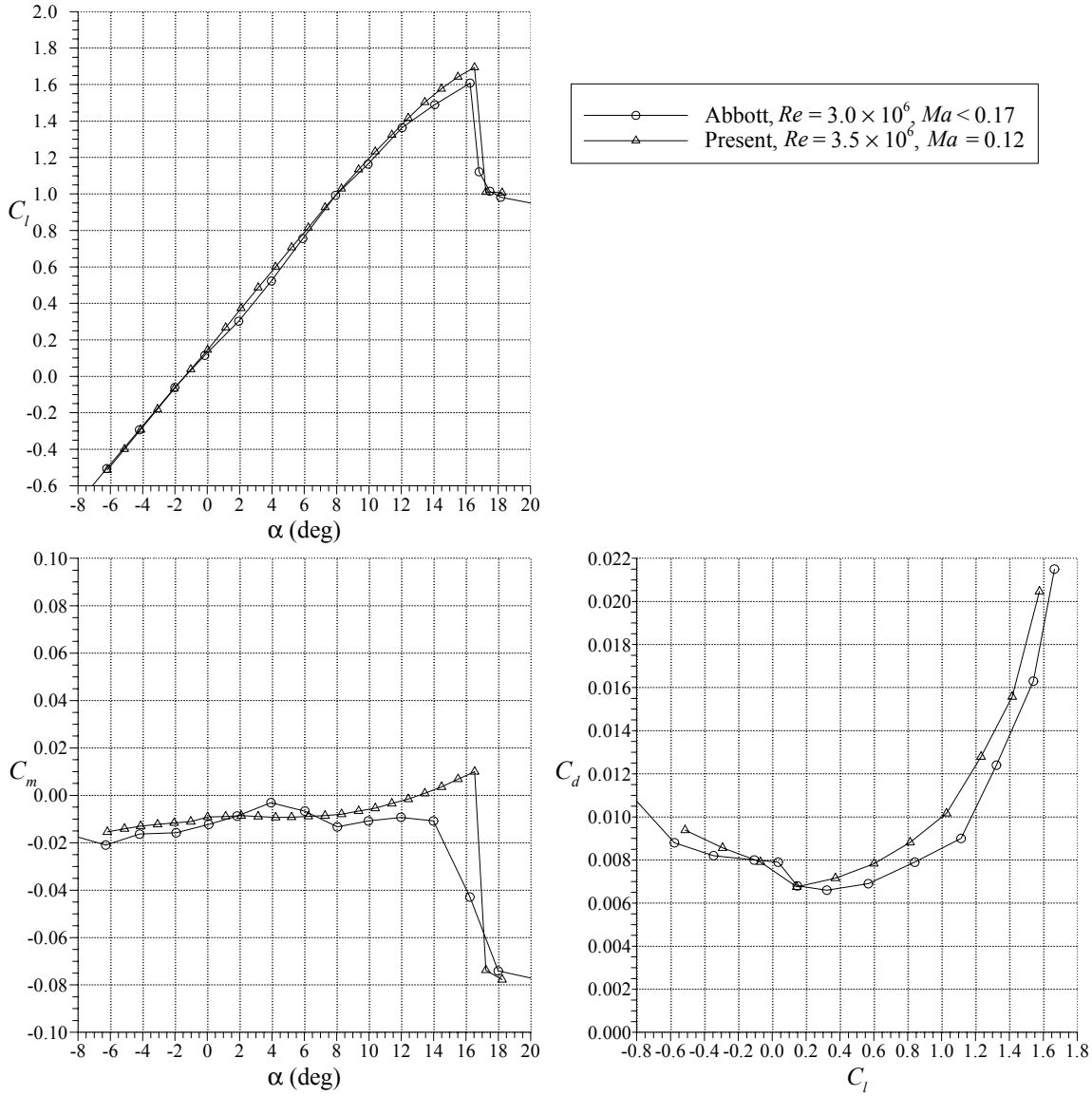

FIGURE 14. COMPARISON OF THE CLEAN NACA 23012 AIRFOIL PERFORMANCE AT $Re = 3.5 \times 10^6$ WITH HISTORICAL DATA FROM ABBOTT AND VON DOENHOFF AT $Re = 3.0 \times 10^6$

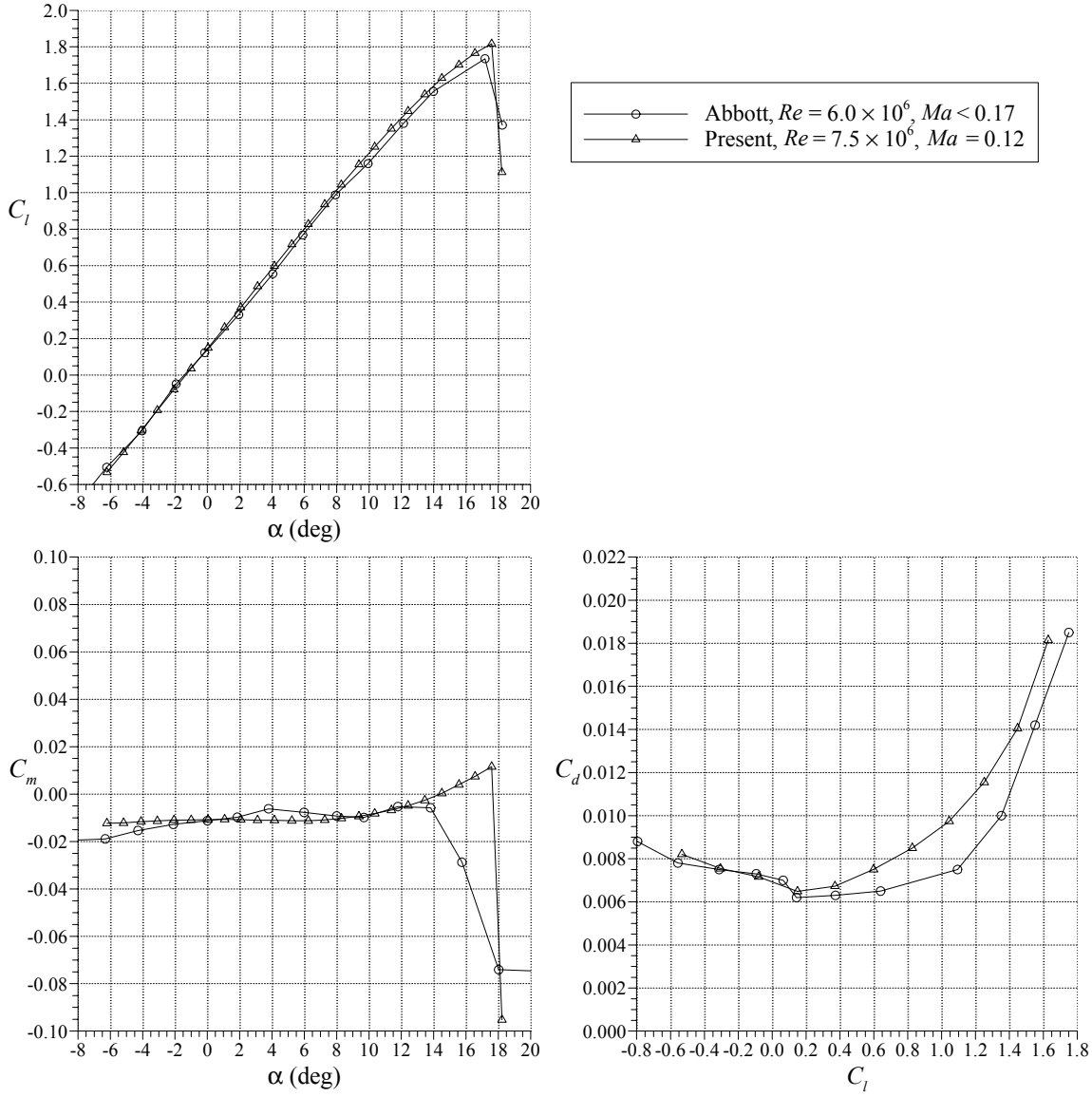

FIGURE 15. COMPARISON OF THE CLEAN NACA 23012 AIRFOIL PERFORMANCE AT $Re = 7.5 \times 10^6$ WITH HISTORICAL DATA FROM ABBOTT AND VON DOENHOFF AT $Re = 6.0 \times 10^6$

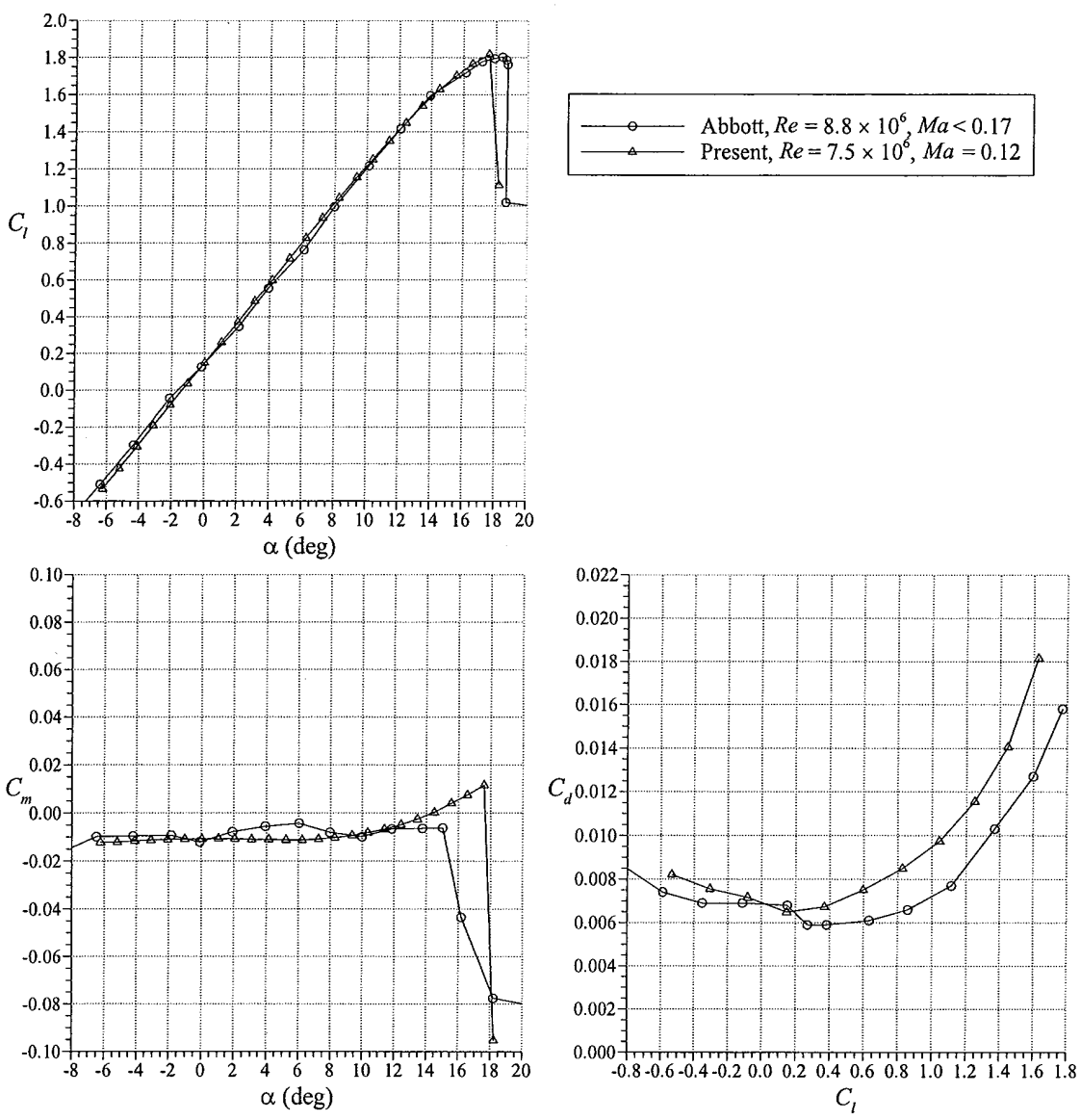

FIGURE 16. COMPARISON OF THE CLEAN NACA 23012 AIRFOIL PERFORMANCE AT $Re = 7.5\times10^6$ WITH HISTORICAL DATA FROM ABBOTT AND VON DOENHOFF AT $Re = 8.8\times10^6$

These trends are nearly identical to the data presented in figures 15 and 16. The only exception was that the historical $C_{l,max}$ data compared more favorably with the present data at higher Reynolds number. In figure 15, the historical data at $Re = 6.0\times10^6$ and $Ma < 0.17$ are compared to the present data at $Re = 7.5\times10^6$ and $Ma = 0.12$. The same Re and Ma values were used in figure 16 for comparison to the Abbott and von Doenhoff data at $Re = 8.8\times10^6$ and $Ma < 0.17$, where the $C_{l,max}$ values for the present and historical data were virtually identical. The α_{stall} was at least one degree larger than the present data. However, this may be due to the smaller angle-of-attack increments given in the historical data. If the present data had been acquired in similar

increments, there may have been better agreement in α_{stall}. Since the present data showed little difference in $C_{l,max}$ between $Re = 7.5\times10^6$ and $Re = 10.5\times10^6$ (for $Ma = 0.12$), using the higher Re data did not affect the comparison between the present and historical data. Overall, these comparisons between the lift coefficients illustrate the reasonable quality of the Abbott and von Doenhoff data, especially given the obvious technical limitations at that time.

Boundary-layer trips were applied to the clean airfoil to promote transition at known locations, $x/c = 0.02$ on the upper surface and $x/c = 0.05$ on the lower surface. The purpose of this was to generate a data set that could be used for comparison to results from other facilities and/or computations. In general, the effect of the trips was minimal on the lift and pitching moment. As expected, the trips caused an increase in drag over the entire angle of attack range. These effects are illustrated in figure 17 for $Re = 7.5\times10^6$ and $Ma = 0.21$.

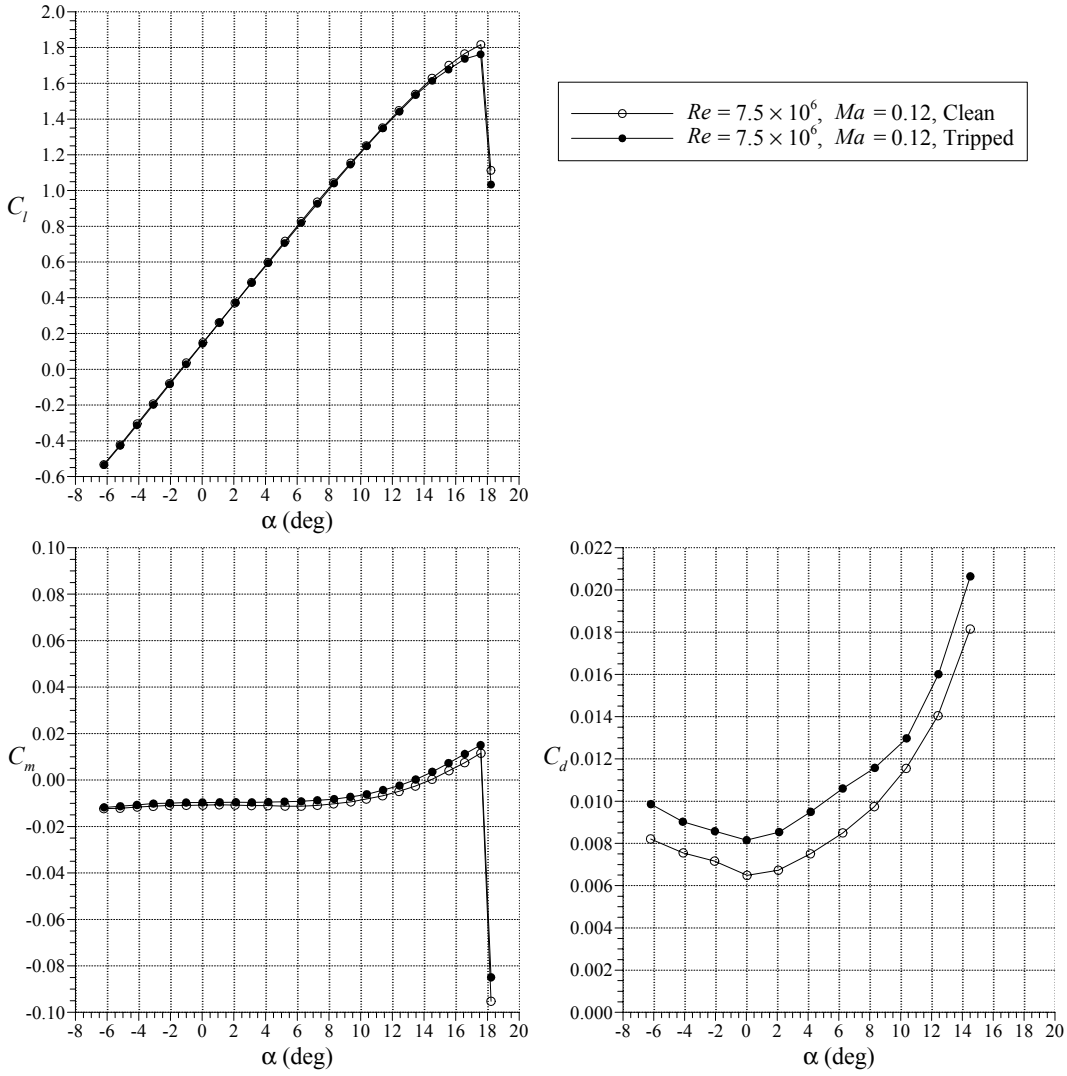

FIGURE 17. EFFECT OF UPPER (AT $x/c = 0.02$) AND LOWER (AT $x/c = 0.05$) SURFACE BOUNDARY-LAYER TRIPS ON THE PERFORMANCE OF THE NACA 23012 AIRFOIL

3.3.2 Iced Airfoil Results.

The performance penalties due to the intercycle ice shapes were found to be very severe. This is illustrated in figure 18 for $Re = 7.5\times10^6$ and $Ma = 0.21$. The decrease in $C_{l,max}$ was 50% or more of the clean value. This was true even for ice shape 322, which resulted from 1-minute boot cycles in rime icing conditions. For the airfoil with the other shapes, the maximum lift was nearly the same ($0.65 < C_l < 0.75$), despite the differences in the ice shape geometry and cloud conditions. The drag data showed that at least a three-fold increase in the minimum C_d for ice shapes 290, 296, and 312. The ice shape 322 case had a smaller increase in drag, probably because the shape was smaller (1-minute cycles) and smoother.

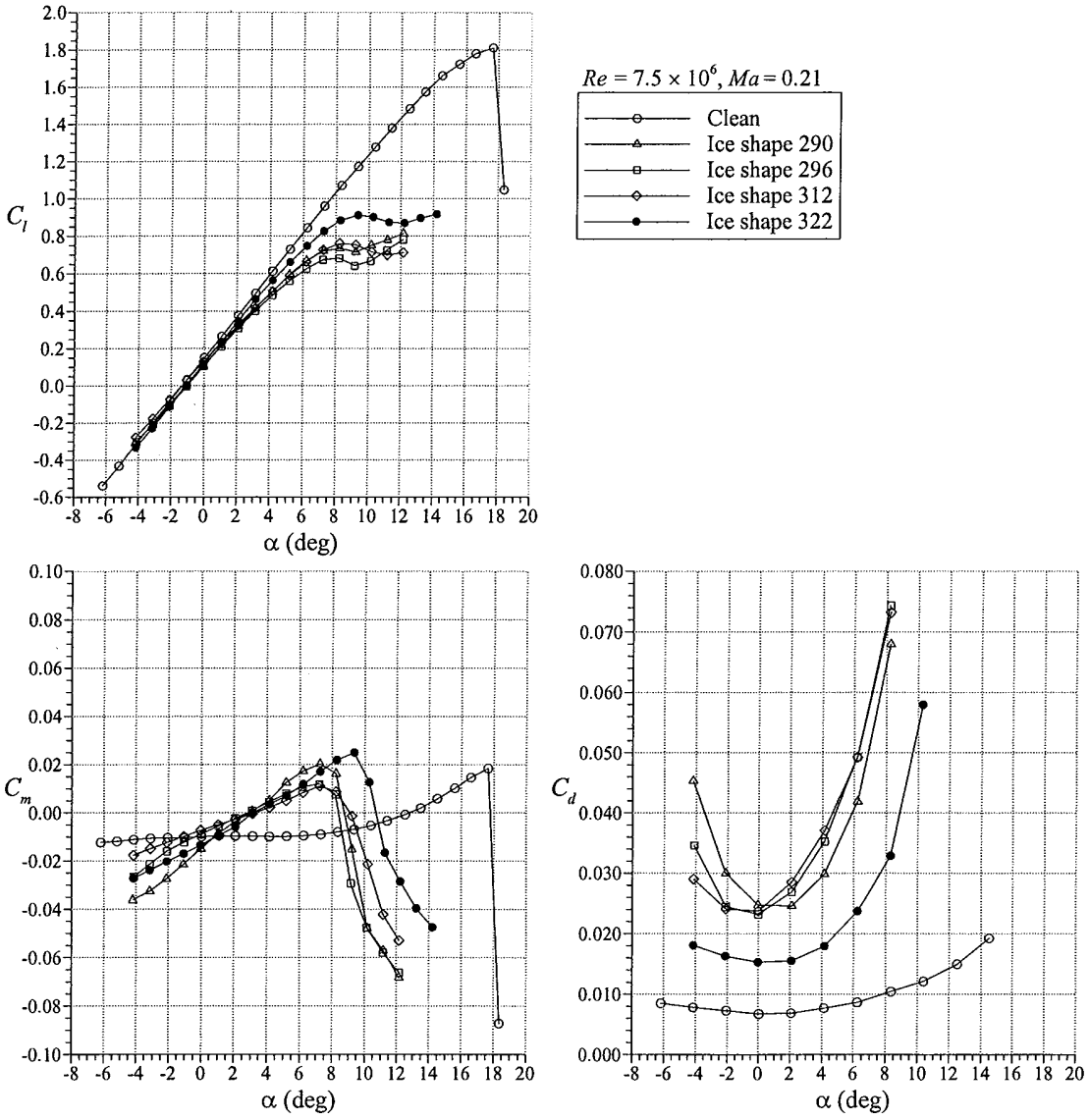

FIGURE 18. PERFORMANCE DEGRADATION DUE TO THE INTERCYCLE ICE SHAPES ON THE NACA 23012 AIRFOIL

The large degradation in the maximum lift coefficient for these ice shapes was likely related to the pressure distribution on the NACA 23012 airfoil. Since the clean airfoil had a large suction peak near the leading edge, the airfoil was more sensitive to protuberances in this region. This is illustrated in figure 19 which compares the pressure distribution on the clean airfoil to that with ice shape 290. The data are for a 9° angle of attack and show how the suction pressures were reduced due to the presence of the ice shape. It is likely that an airfoil with a more gradual pressure recovery would have less severe lift degradation due to a similar ice shape. This idea is explained in more detail by Lee [15] and Lee, et al. [1, 16].

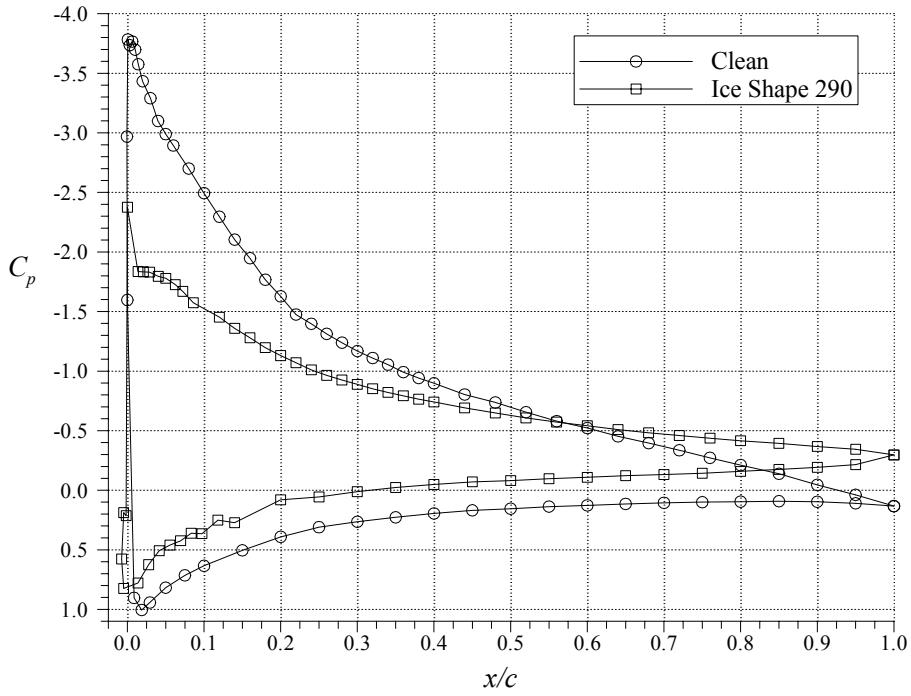

FIGURE 19. COMPARISON OF CLEAN AND ICED PRESSURE DISTRIBUTIONS FOR THE NACA 23012 AIRFOIL AT $\alpha = 9°$, $Re = 7.5\times10^6$, AND $Ma = 0.21$

The effect of Reynolds and Mach number variation was also explored for all of the ice shapes. An example of these effects is shown in figures 20 through 22 for ice shape 290. The data in figure 20 show that there was virtually no variation in the lift with increasing Reynolds number at constant Mach number. The drag behavior was more similar to the clean case with a decrease in C_d from $Re = 3.5\times10^6$ to $Re = 7.5\times10^6$, over the linear lift range. Figures 21 and 22 show that there was a measurable variation in $C_{l,max}$ with Mach number at constant Reynolds number. This trend is similar to the clean case, where the $C_{l,max}$ decreased with increasing Mach number. However, this difference is very small relative to the overall performance degradation due to the ice shape. The drag behavior was also very similar to the clean case, where the C_d values were generally higher for higher Mach numbers.

The Reynolds and Mach number behavior is also plotted for ice shape 322. Recall that the performance degradation for this shape was slightly less severe than for the other three (cf. figure 18). Despite this, the Reynolds and Mach number trends shown in figures 23 and 24 were

nearly identical to that described for ice shape 290. Although not shown here, these trends were also observed for the other two ice shapes. Furthermore, the data from runs performed at $Re = 2.0\times10^6$ and $Ma = 0.095$ (with the ice shapes attached) showed little deviation from the higher Reynolds and Mach number cases. An important conclusion is that the iced airfoil performance coefficients dependence upon Reynolds and Mach numbers is minor relative to the degradation from the clean values. This is consistent with results from other studies [17, 18] using different airfoils with different types of ice accretions and may be indicative of a general trend in the aerodynamics of iced airfoils.

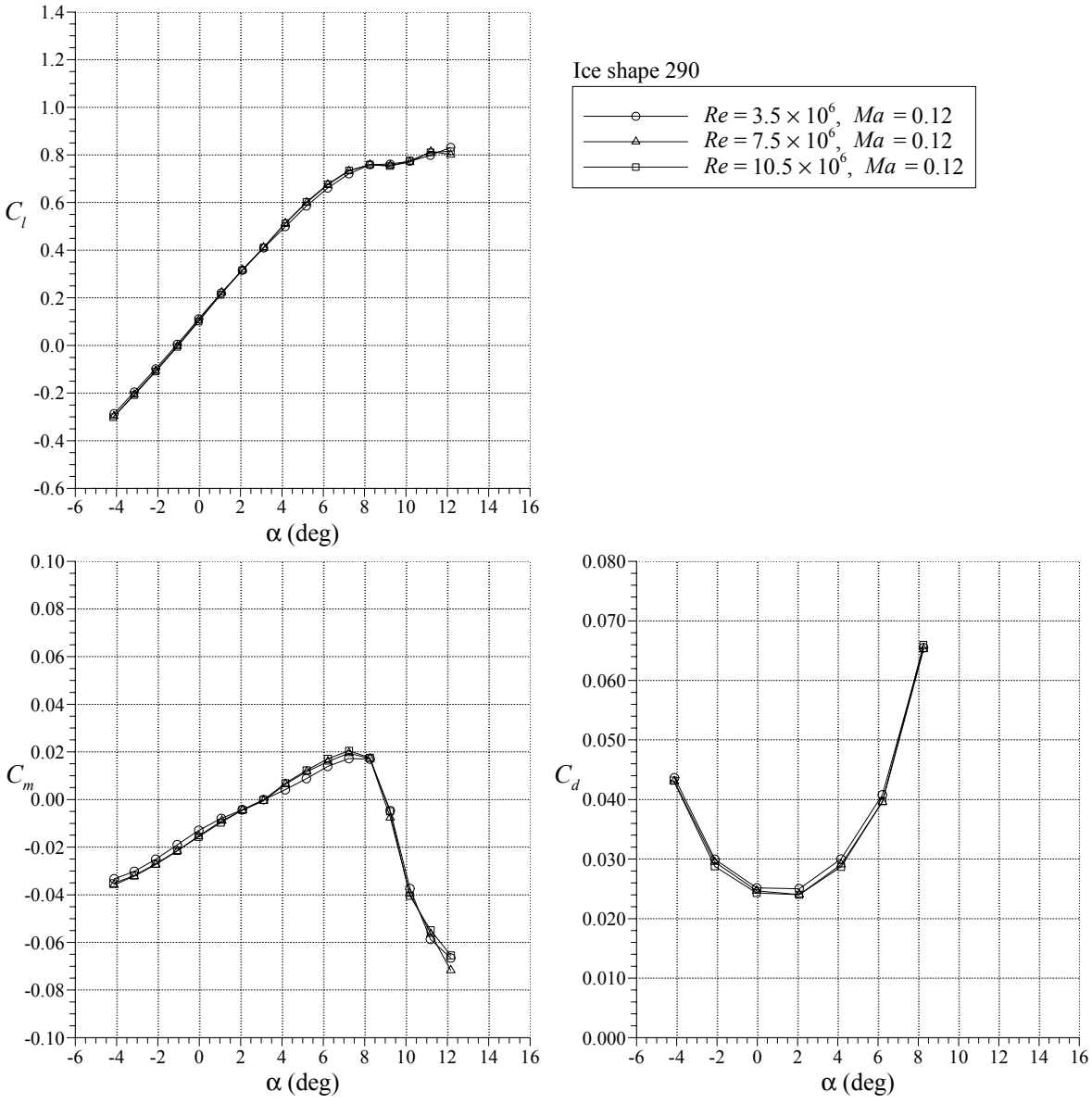

FIGURE 20. EFFECT OF REYNOLDS NUMBER AT CONSTANT MACH NUMBER ON THE PERFORMANCE OF THE NACA 23012 AIRFOIL WITH ICE SHAPE 290

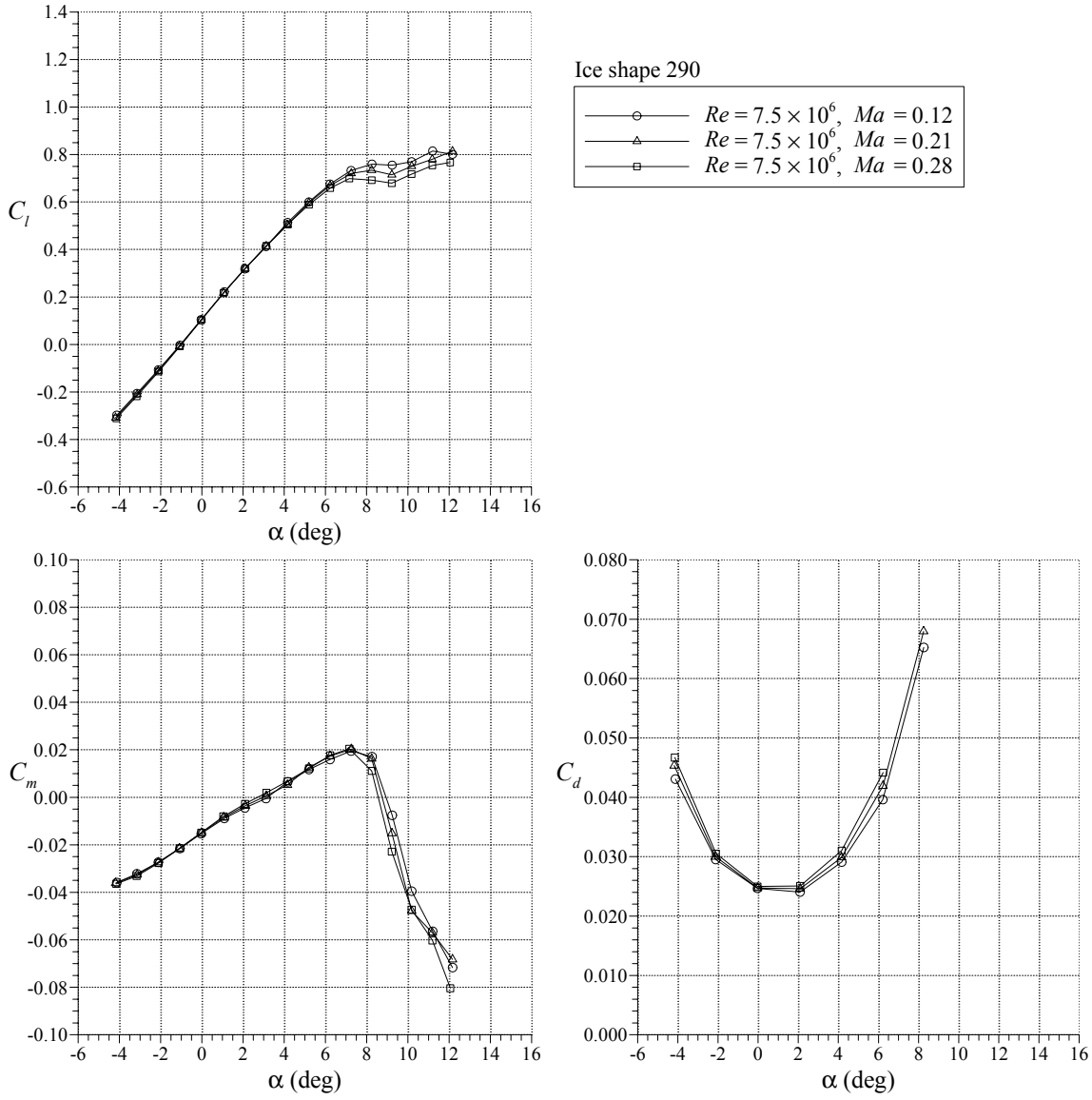

FIGURE 21. EFFECT OF MACH NUMBER AT CONSTANT REYNOLDS NUMBER OF 7.5×10^6 ON THE PERFORMANCE OF THE NACA 23012 AIRFOIL WITH ICE SHAPE 290

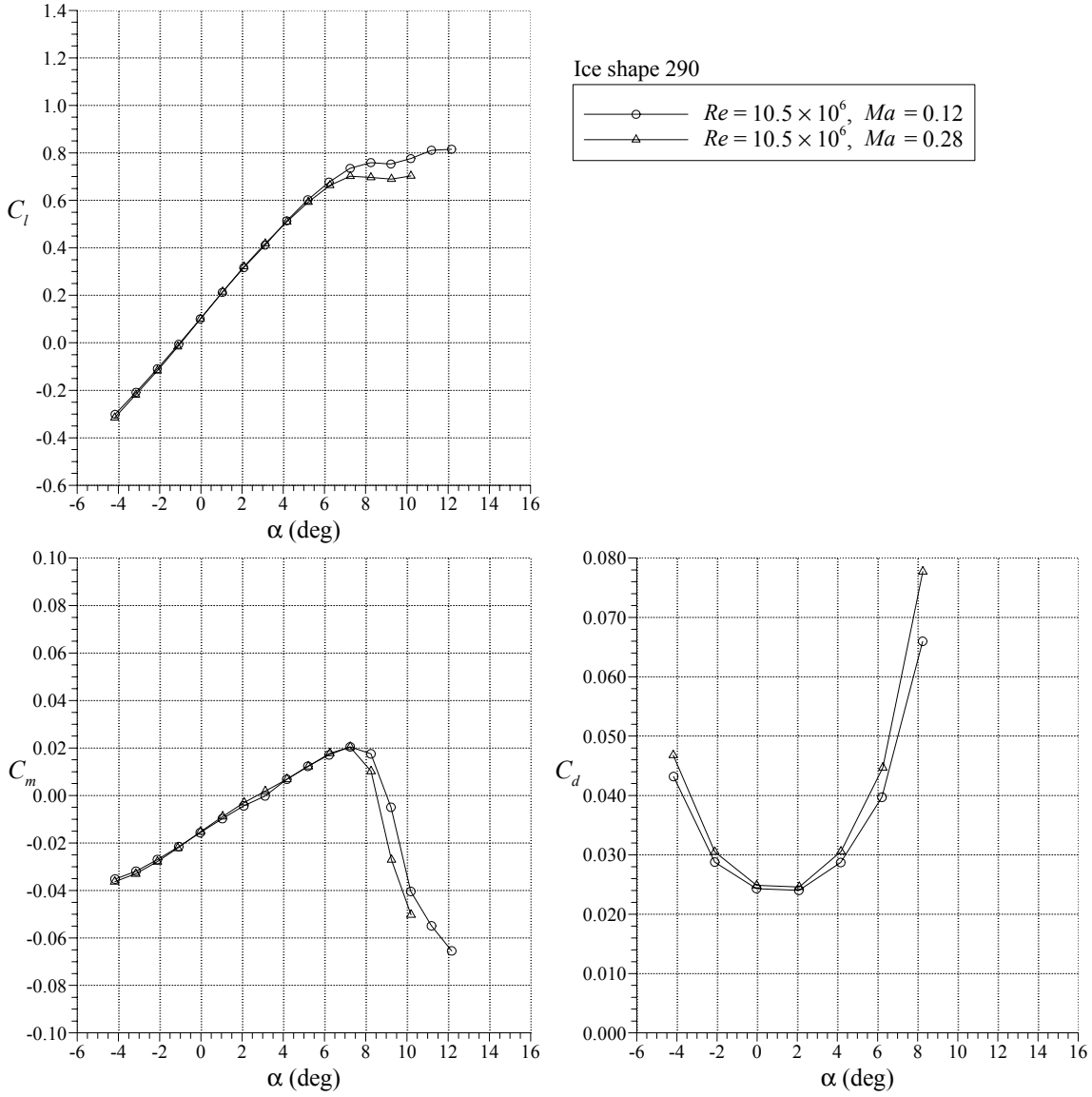

FIGURE 22. EFFECT OF MACH NUMBER AT CONSTANT REYNOLDS NUMBER OF 10.5×10^6 ON THE PERFORMANCE OF THE NACA 23012 AIRFOIL WITH ICE SHAPE 290

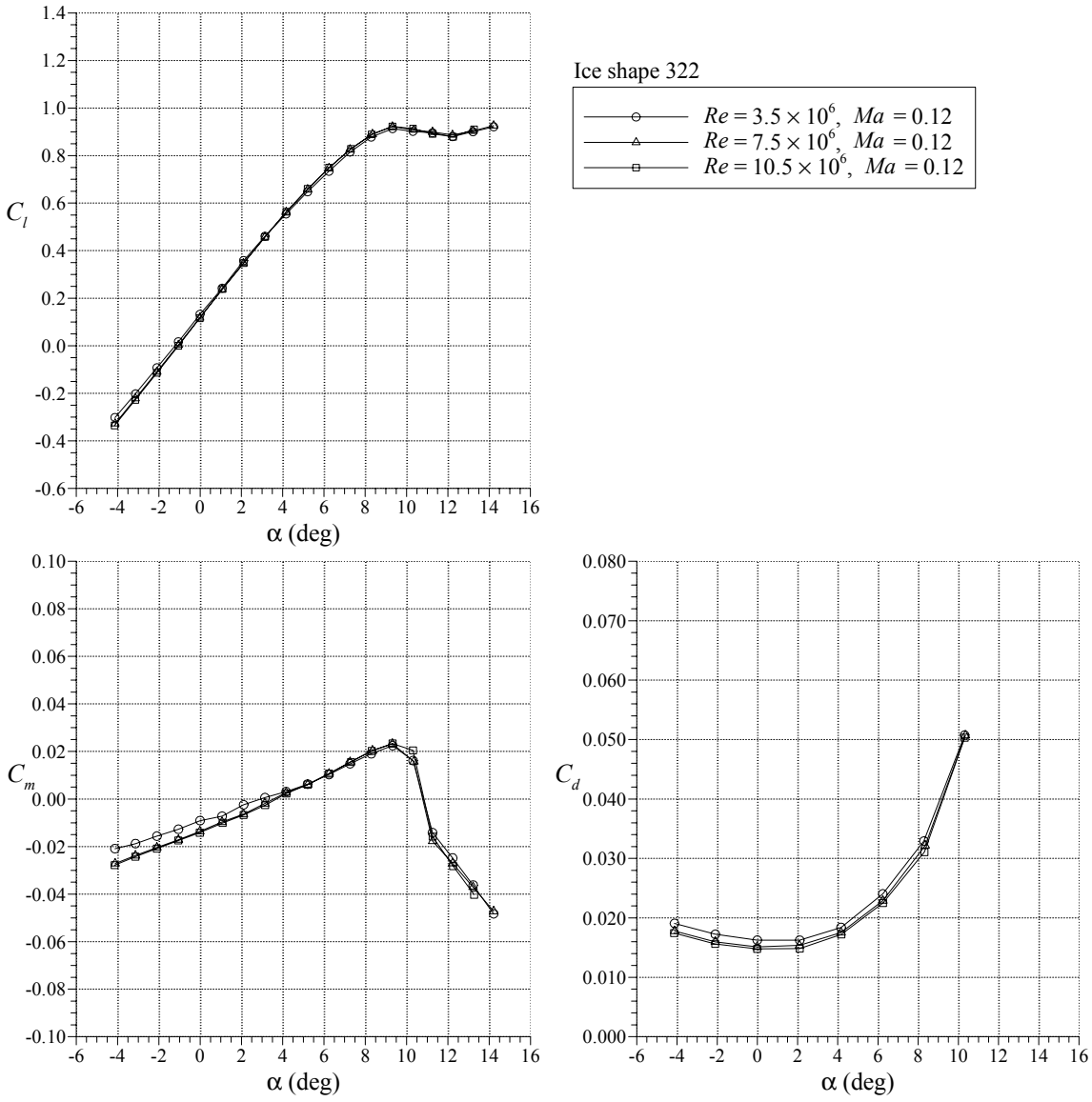

FIGURE 23. EFFECT OF REYNOLDS NUMBER AT CONSTANT MACH NUMBER ON THE PERFORMANCE OF THE NACA 23012 AIRFOIL WITH ICE SHAPE 322

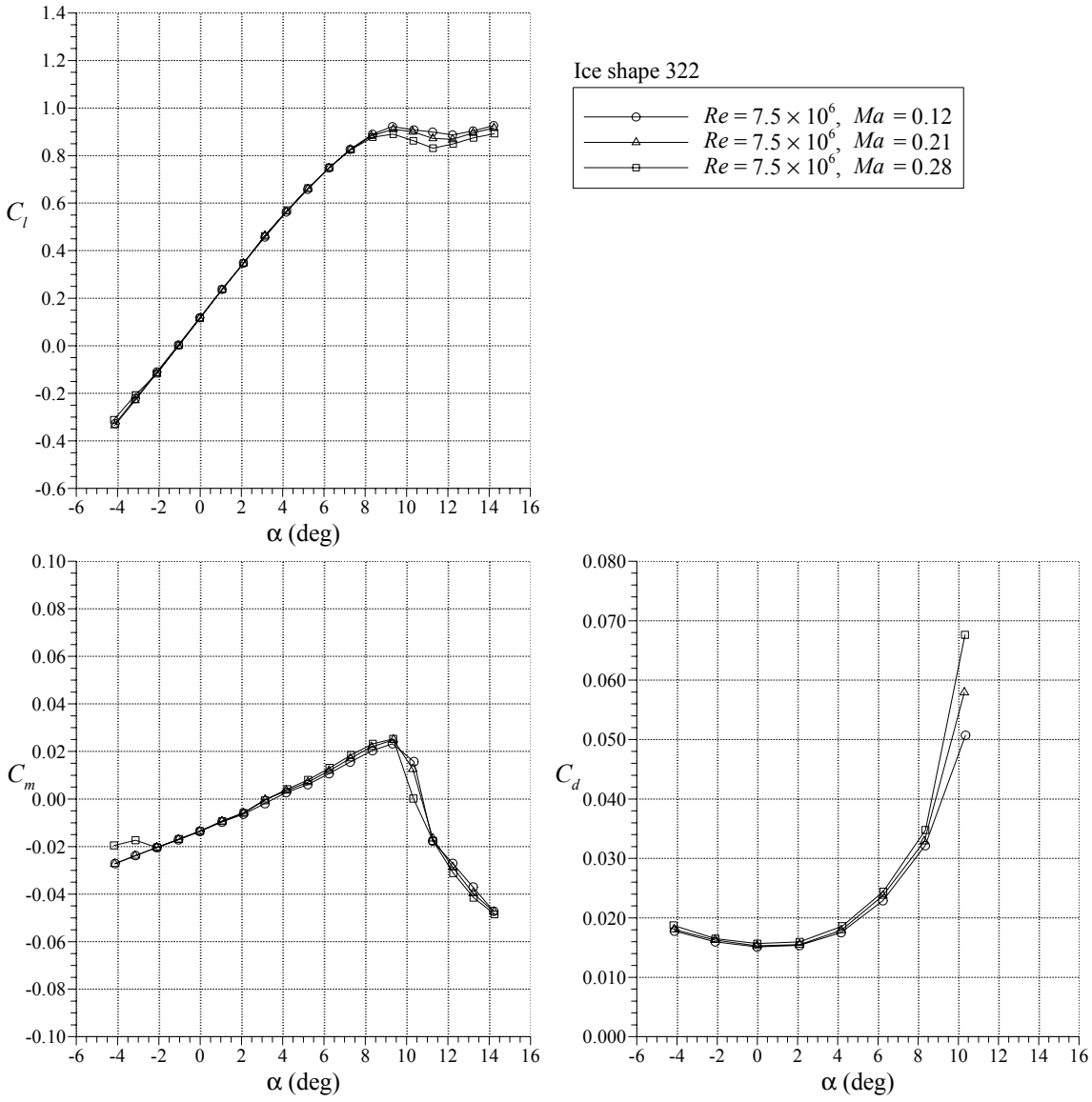

FIGURE 24. EFFECT OF MACH NUMBER AT CONSTANT REYNOLDS NUMBER ON THE PERFORMANCE OF THE NACA 23012 AIRFOIL WITH ICE SHAPE 322

The NACA 23012 airfoil section was also tested with 40- and 80-grit sandpaper applied to the leading edge. This was an attempt to find a standard type of roughness that would cause performance degradation similar to the actual intercycle ice accretions. It also provides a standard form of roughness that can be used to compare data from other facilities. Figure 25 shows that the performance of the airfoil with the sandpaper was degraded from the clean case but was still significantly better than for the ice accretions. The performance penalty in $C_{l,max}$ was about 25% as opposed to about 60% for the ice accretion castings. The drag values for the airfoil with sandpaper were closer to the clean values than to the ice accretion values.

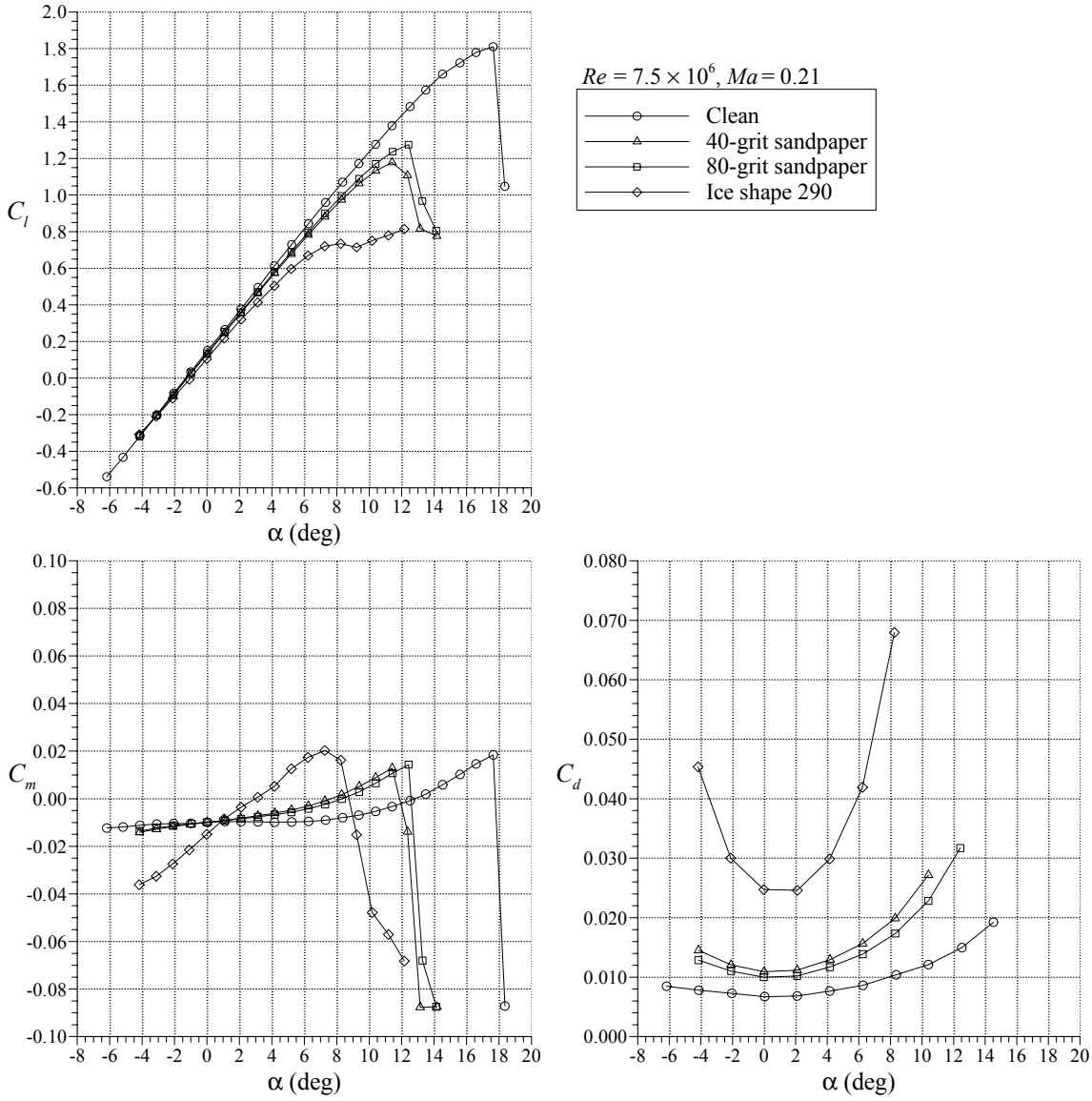

FIGURE 25. PERFORMANCE DEGRADATION DUE TO THE 40- AND 80-GRIT SANDPAPER ON THE NACA 23012 AIRFOIL

A side-by-side comparison of the intercycle ice accretions and the sandpaper reveals that their geometries are not very similar. The sandpaper had a very uniform array of roughness, whereas the cast ice shapes contained ridge-like features that were not uniform, especially in the spanwise direction. The effect of these ridge-like features was local boundary-layer separation on the airfoil upper surface, particularly near maximum lift. This was discussed above in connection with figure 19. The sandpaper, being more uniform, did not cause similar separation to occur and the peak suction was mostly maintained. This is illustrated in figure 26 where the general shapes of the clean and 40-grit sandpaper pressure distributions were very similar. Another factor was that even the larger roughness (40 grit) was considerably smaller in size than the actual accretions. For example, the nominal height (ignoring the larger ridge-like features) of the ice shape 290 had a normalized height (k/c) on the order of 0.0056, while the normalized height of the 40-grit sandpaper was nearly five times smaller at $k/c = 0.0012$.

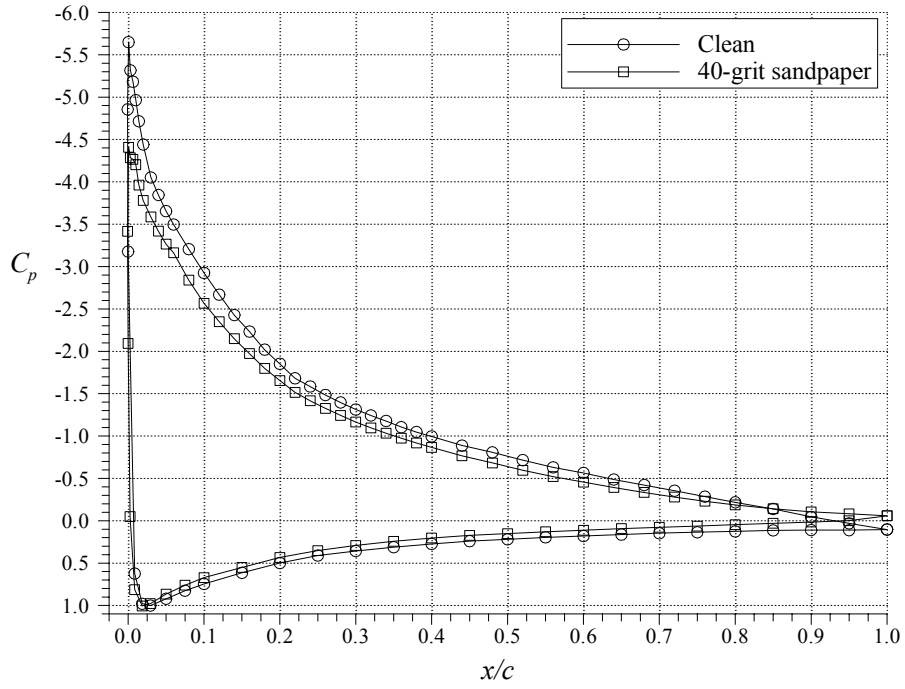

FIGURE 26. COMPARISON OF CLEAN AND 40-GRIT SANDPAPER PRESSURE DISTRIBUTIONS FOR THE NACA 23012 AIRFOIL AT $\alpha = 11°$, $Re = 7.5\times10^6$, AND $Ma = 0.21$

The effect of Reynolds and Mach numbers on performance was also investigated for both the 40- and 80-grit sandpaper cases. These data are summarized in figures 27 through 30 and the results were similar to that for the ice shapes. The Reynolds number change had virtually no effect on the lift and pitching moment curves for the airfoil with 40-grit sandpaper (figure 27). The drag decreased at the higher Reynolds numbers. The change in Mach number caused a slight reduction in $C_{l,max}$ between $Ma = 0.12$ and $Ma = 0.21$, but there were larger effects on the pitching moment and drag (figure 28). The results for the 80-grit sandpaper were slightly different in that the Reynolds number change did have a slight effect on the lift curve and more of an effect on the drag than for the 40-grit sandpaper (figure 29). On the other hand, the Mach number had virtually no effect on $C_{l,max}$ for the 80-grit sandpaper, but the effects on the pitching moment and drag were typical (figure 30).

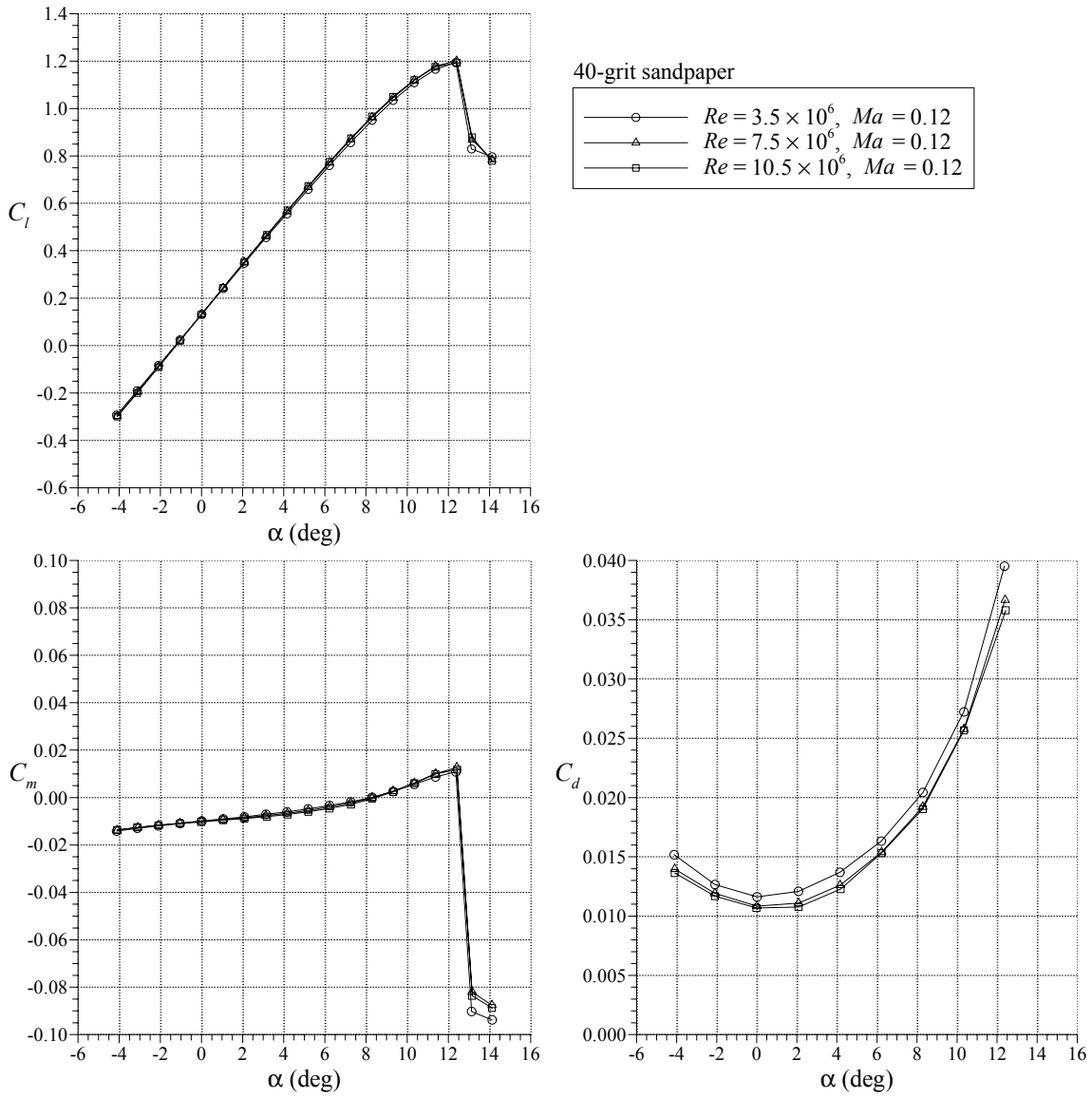

FIGURE 27. EFFECT OF REYNOLDS NUMBER AT CONSTANT MACH NUMBER ON THE PERFORMANCE OF THE NACA 23012 AIRFOIL WITH 40-GRIT SANDPAPER

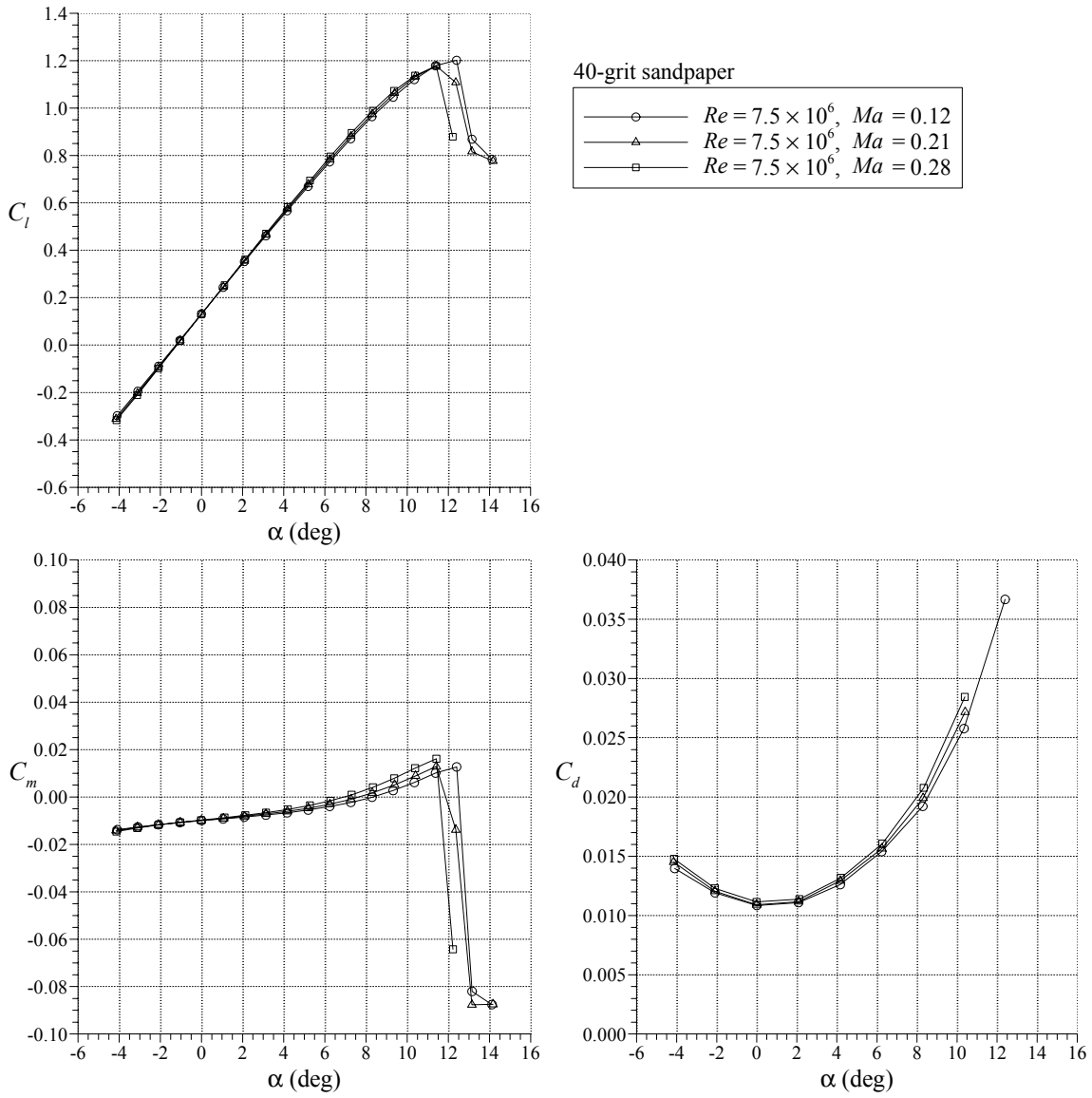

FIGURE 28. EFFECT OF MACH NUMBER AT CONSTANT REYNOLDS NUMBER ON THE PERFORMANCE OF THE NACA 23012 AIRFOIL WITH 40-GRIT SANDPAPER

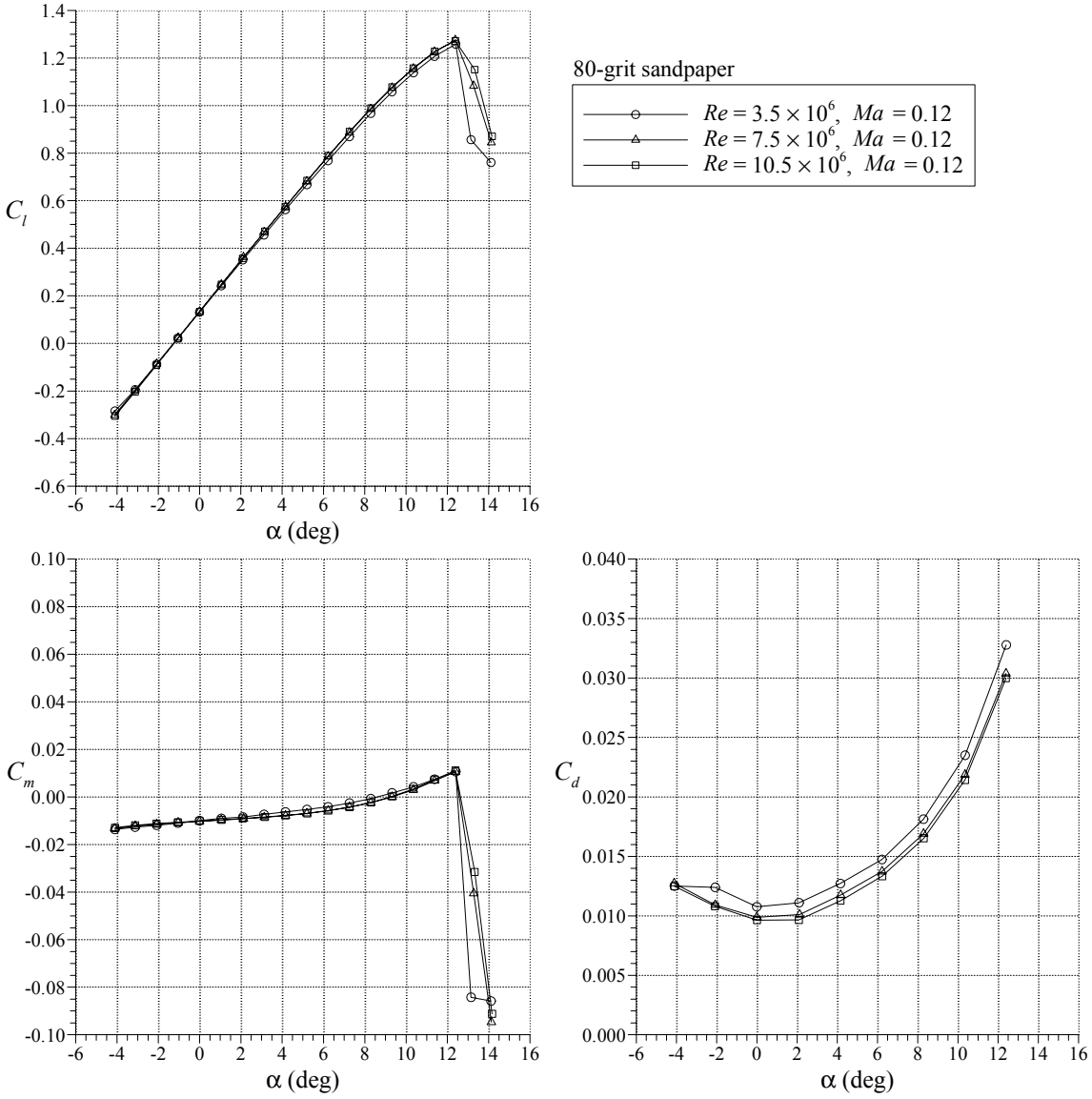

FIGURE 29. EFFECT OF REYNOLDS NUMBER AT CONSTANT MACH NUMBER ON THE PERFORMANCE OF THE NACA 23012 AIRFOIL WITH 80-GRIT SANDPAPER

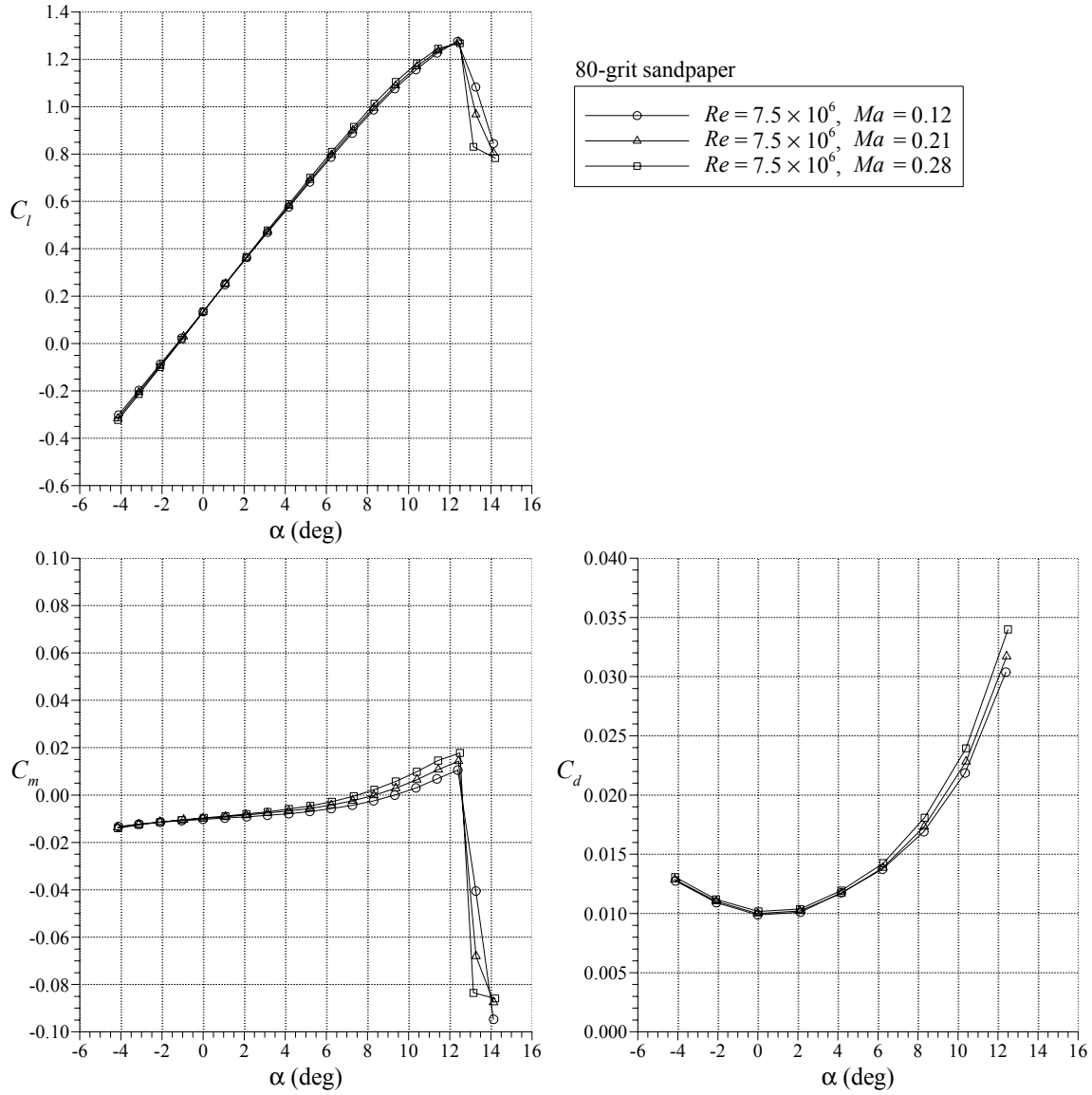

FIGURE 30. EFFECT OF MACH NUMBER AT CONSTANT REYNOLDS NUMBER ON THE PERFORMANCE OF THE NACA 23012 AIRFOIL WITH 80-GRIT SANDPAPER

4. SUMMARY, CONCLUSIONS, AND RECOMMENDATIONS.

4.1 SUMMARY.

Ice accretion testing was carried out on a NACA 23012 airfoil section which had a 36-inch chord and was equipped with a pneumatic deicer. The icing runs were performed at several different cloud conditions modeled after FAR 25 Appendix C. The Reynolds and Mach numbers were 6.5×10^6 and 0.27, respectively (for 14°F static temperature). Residual and intercycle ice shapes were generated at 0° and 4° angle of attack. The deicing boots were cycled several times during each run to ensure that a steady state was achieved. Repeat runs were performed to verify that

the documented ice shapes were representative of the test condition and not anomalies. The residual and intercycle ice accretions were documented for all runs using standard techniques such as tracings and photographs. For selected intercycle shapes, molds were made of the accretions and were later converted into castings for aerodynamic testing.

The aerodynamic performance testing was carried out using a similar 36-inch chord NACA 23012 airfoil model. The model had removable leading edges so that castings of the intercycle ice shapes could be installed in place of the clean leading edge. This simulated the actual ice accretion with high fidelity. The testing was conducted in a pressurized facility so that near-flight Reynolds and Mach numbers (for a typical turbopropeller or piston aircraft) could be independently controlled. A detailed set of measurements was performed for the clean airfoil configuration and then four intercycle ice shapes were tested. Tests were also conducted with standard, uniformly distributed roughness in the form of 40- and 80-grit sandpaper applied to the airfoil leading edge.

4.2 CONCLUSIONS.

The ice accretion testing proved to be very informative for this airfoil and deicing boot. Several conclusions were made. The spray times and number of boot cycles chosen for these runs (four for continuous maximum cases and three for intermittent maximum cases) were sufficient for the residual and intercycle ice shapes to reach a steady state. This means that the accretions were very similar in size and shape after multiple boot cycles. Overall, the intercycle ice accretions tended to be much larger than the residual ice. This implies that the deicing system was effective in cleaning the leading edge. A large amount of ice did build up before the next cycle—3 minutes for the continuous maximum cases. The intercycle ice shapes for the intermittent maximum cases were generally smaller, owing to the 1-minute cycles, despite the higher water loading. A single continuous maximum condition was run with 1-minute boot cycles, and this was found to be very effective in both cleaning the leading edge and minimizing the size of the intercycle ice accretion. Also, it was found that decreasing the initial activation time did not substantially affect the resulting intercycle ice shape. This means that the boots were just as effective when they were activated 11 seconds after the start of the spray as when they were activated after a quarter-inch of ice was allowed to accrete (252 seconds) on the leading edge, for the one condition tested. The intercycle accretions selected for aerodynamic testing tended to be larger and were selected as the "worst case scenario." These accretions tended to be repeatable from run to run and, therefore, were not anomalies.

Aerodynamic testing of the clean NACA 23012 airfoil yielded several important conclusions as well. Paramount of these was the importance of distinguishing between Reynolds and Mach number effects. For example, there was a significant decrease in maximum lift and stall angle with increasing Mach number at constant Reynolds number. On the other hand, there was a significant increase in maximum lift from $Re = 3.5\times10^6$ to $Re = 7.5\times10^6$ at a constant Mach number of 0.12. This illustrates that both Reynolds and Mach number effects are important in comparing data from different facilities. In addition, the clean data presented here compare favorably with historical data for the NACA 23012 airfoil.

The intercycle ice shapes caused a significant performance degradation. Maximum lift values were typically reduced from 1.8 (clean) to 0.7 (iced) and stall angle values were reduced from

17° (clean) to 9° (iced). The minimum drag coefficient increased from 0.007 (clean) to 0.026 (iced). An increase in Reynolds number at a constant Mach number of 0.12 had virtually no effect on the lift curve or the stall. Mach number variation at constant Reynolds number had a small effect, decreasing the maximum lift with increasing Mach number. These results imply that smaller scale testing of similar ice shapes in atmospheric facilities may be a very cost-effective and worthwhile approach. Still, care must be taken in analyzing "Reynolds number trends," since it appears that Mach number plays a more signal role in the performance coefficient variations for the airfoil and ice shapes tested.

The 40- and 80-grit sandpaper was not adequate in simulating the intercycle ice shape performance degradation. Maximum lift values were typically reduced from 1.8 (clean) to 1.2 (sandpapered) and stall angles were reduced from 17° (clean) to 12° (sandpapered). The minimum drag coefficient increased from 0.007 (clean) to 0.011 (sandpapered). The sandpaper roughness was not large enough to accurately simulate even the nominal heights of the intercycle shapes, as it was smaller by a nearly a factor of five. Additionally, the sandpaper did not have ridge-like features comparable to the actual accretions.

4.3 RECOMMENDATIONS.

There is a recommendation that followed directly from the ice accretion testing and concerns the operation of the pneumatic deicer. For the one case (continuous maximum condition) that was tested, initiating the boot operation as soon as icing was detected and using a 1-minute cycle (i.e., instead of a 3-minute cycle) was most effective in limiting the size of the residual and intercycle accretions. Direct observation of the deicer operation during other runs indicated that this approach may work equally well for other cloud conditions. Therefore, this "early and often" approach should be given more consideration as a means of limiting the size of residual and intercycle ice accretions, either in actual flight operations or in future testing.

The other recommendations result from the combined conclusions of the entire study. The very large performance degradation associated with the intercycle ice shapes implies that a more detailed study may be warranted. A remaining question is what effect scale has on ice accretion geometry. The 36-inch chord models used in this study were not representative of a typical wing chord. Reasonable questions may arise about how the present data would apply to characteristics and resulting performance degradation of ice accretions obtained on a larger scale model. This would primarily affect the ice accretion geometry, since this study has shown that Reynolds and Mach number effects on performance are very small in the iced case. Since ice accretions and pneumatic boot operation cannot be scaled reliably, full-scale intercycle ice accretions need to be acquired and tested to confirm the aerodynamic performance degradation observed in this study. The effect of airfoil geometry should also be considered. Previous research has shown that the NACA 23012 airfoil is very sensitive to leading-edge type ice accretions. Therefore, it is important to determine the performance degradation of similar intercycle ice shapes on other airfoils. This could be done on a smaller scale provided a reasonable scaling and simulation method was used.

5. REFERENCES.

1. Lee, S., Kim, H.S., and Bragg, M.B., "Investigation of Factors that Influence Iced-Airfoil Aerodynamics," AIAA Paper 2000-0099, January 2000.

2. Shin, J., and Bond, T.H., "Surface Roughness Due to Residual Ice in the Use of Low Power Deicing Systems," NASA TM-105971, AIAA Paper 93-0031, January 1993.

3. Albright, A.E., Kohlman, D.L., Schweikhard, W.G., and Evanich, P., "Evaluation of a Pneumatic Boot Deicing System on a General Aviation Wing Model," NASA TM-82363, June 1981.

4. Bowden, D.T., "Effect of Pneumatic De-Icers and Ice Formations on Aerodynamic Characteristics of an Airfoil," NACA TN-3564, February 1956.

5. Reichhold, J.D. and Bragg, M.B., "Residual Ice Characteristics and the Resulting Aerodynamic Performance Penalties," NASA AGATE WP4.010, University of Illinois at Urbana-Champaign, May 1998.

6. Jackson, D.G. and Bragg, M.B., "Aerodynamic Performance of an NLF Airfoil With Simulated Ice," AIAA Paper 99-0373, January 1999.

7. Hill, E.G., "Airplane Deicing Ice Protection Systems, Deicing Boot Ice Bridging, and Airplane Operating Procedures During In-Flight Icing Conditions," Federal Aviation Administration Transportation Airplane Directorate, February 1999.

8. Hill, E.G. and Reehorst, A.L. (eds.), "FAA/NASA Deicing Boot Ice Bridging Workshop Proceedings," Ohio Aerospace Institute, Cleveland, OH, November 19, 1997.

9. Riley, J.T., Rios, M.A., Anderson, D., and Dumont, C.J., "A Study of Intercycle, Residual and Pre-Activation Ice," AIAA Paper 2001-0089, January 2001.

10. Broeren, A.P., Addy, H.E., Jr., and Bragg, M.B., "Effect of Intercycle Ice Accretions on Airfoil Performance," AIAA Paper 2002-0240, January 2002.

11. Pascal, K., Goodman, W., McGee, R., Walker, B., and Wilcox, P.A., "Evaluation of Tunnel Sidewall Boundary-Layer-Control Systems for High-Lift Airfoil Testing," AIAA Paper 91-3243, 9th Applied Aerodynamics Conference, Baltimore, MD, September 23-25, 1991.

12. Allen, H.J. and Vincenti, W.G., "Wall Interference in a Two-Dimensional Flow Wind Tunnel, With Consideration of the Effect of Compressibility," NACA Report No. 782, 1944.

13. Ladson, C.L., "Effects of Independent Variation of Mach and Reynolds Numbers on the Low-Speed Aerodynamic Characteristics of the NACA 0012 Airfoil Section," NASA TM-4071, October 1988.

14. Abbot, I.H. and von Doenhoff, A.E., *Theory of Wing Sections*, Dover Publications, pp. 124-128 and 498-499, 1959.
15. Lee, S., "Effect of Supercooled Large Droplet Icing on Airfoil Aerodynamics," Ph.D. Dissertation, Dept. of Aeronautical and Astronautical Engineering, Univ. of Illinois, Urbana, IL, 2001.

16. Lee, S. and Bragg, M.B., "Effects of Simulated-Spanwise Ice Shapes on Airfoils: Experimental Investigation," AIAA Paper 99-0092, January 1999.

17. Addy, H.E., Jr. and Chung, J.J., "A Wind Tunnel Study of Icing Effects on a Natural Laminar Flow Airfoil," AIAA Paper 2000-0095, January 2000.

18. Morgan, H.L., Jr., Ferris, J.C., and McGhee, R.J., "A Study of High-Lift Airfoils at High Reynolds Numbers in the Langley Low-Turbulence Pressure Tunnel," NASA TM 89125, July 1987.

APPENDIX A—SIDEWALL VENTING EFFECTS

The effect of sidewall venting on both the clean and iced airfoil performance was found to be small. This is especially true relative to the effect of the intercycle ice accretions on the airfoil performance. The purpose of this appendix is to present some of the no-venting data so as to justify these conclusions. While it is true that the Low-Turbulence Pressure Tunnel venting system was not specifically designed nor optimized for the present test, the data presented here show that the effect is small enough to mitigate this concern.

A.1 Clean Airfoil Data.

The effect of sidewall venting on the clean airfoil data is summarized in figures A-1 and A-2. The data for $Re = 3.5\times10^6$ and $Ma = 0.12$ (figure A-1) show that the lift and pitching moment variation with angle of attack was virtually identical with or without venting. On the other hand, there was a slight difference in the drag coefficients. The reason that the measured drag was lower in the no-venting case is not clear. However, this is a common trend in the sidewall venting comparisons. It is important to note that highly accurate drag measurements were not a chief objective of this study. This difference is small relative to the drag increases due to the intercycle ice shapes.

Figure A-2 shows venting and no-venting data for $Ma = 0.12$ and 0.28 at $Re = 10.5\times10^6$. The lift data again show that there was virtually no difference between the venting and no-venting case. The slight discrepancy for the $Ma = 0.12$ stalling angle may be related to the angle of attack increments in which the data were acquired. These values may have been closer if smaller increments were used, since the NACA 23012 has a sharp stall characteristic. These comments also apply to the pitching-moment data. The drag data for $Ma = 0.12$ show a similar trend to figure A-1, where the no-venting cases tended to have smaller values. However, the venting and no-venting drag values for the $Ma = 0.28$ case were nearly identical. The minor effect of sidewall venting seen here is further supported by the good agreement between the present and historical data, the latter having been acquired using a 24-inch chord airfoil model.

A.2 Iced Airfoil Data.

The effect of sidewall venting was also found to be small for the airfoil with ice shapes attached. This is summarized in figure A-3, which shows data for ice shape 290. Similar to the clean case, the difference in maximum lift was larger for $Ma = 0.12$, however, the shape of the curves was identical. It is possible that this difference could be partly attributed to typical run-to-run variations, since it is likely that the stalled flow was unsteady. The drag data show trends similar to the clean data, with the exception of the data at $Ma = 0.12$ for angles of attack less than 0°. Here the data with venting had lower drag values than its no-venting counterpart. These minor variations in drag data may be more expected for the iced airfoil, since the wake flow field was likely more three-dimensional and unsteady.

At the risk of being redundant, more venting comparison data is shown in figure A-4 for the airfoil with 80-grit sandpaper applied over the leading edge. Here again, the differences between the lift coefficient data with and without venting was very small. The venting cases had slightly

higher maximum lift coefficients, but the variation with Mach number was preserved. Analogous trends are shown in the drag data as well.

A.3 Summary.

These data illustrate the minor effect of sidewall venting on the clean and iced airfoil results. In terms of the lift and pitching moment characteristics the stall behavior was virtually identical with or without venting for most cases. In cases where there was a noticeable difference, the appropriate Mach and Reynolds number trends were still preserved. There was more variation in the drag data between the venting and no-venting cases, but this was relatively small compared to the differences in drag between the clean and iced airfoil cases. Therefore, the effect of sidewall venting does not have any bearing upon the conclusions of this report.

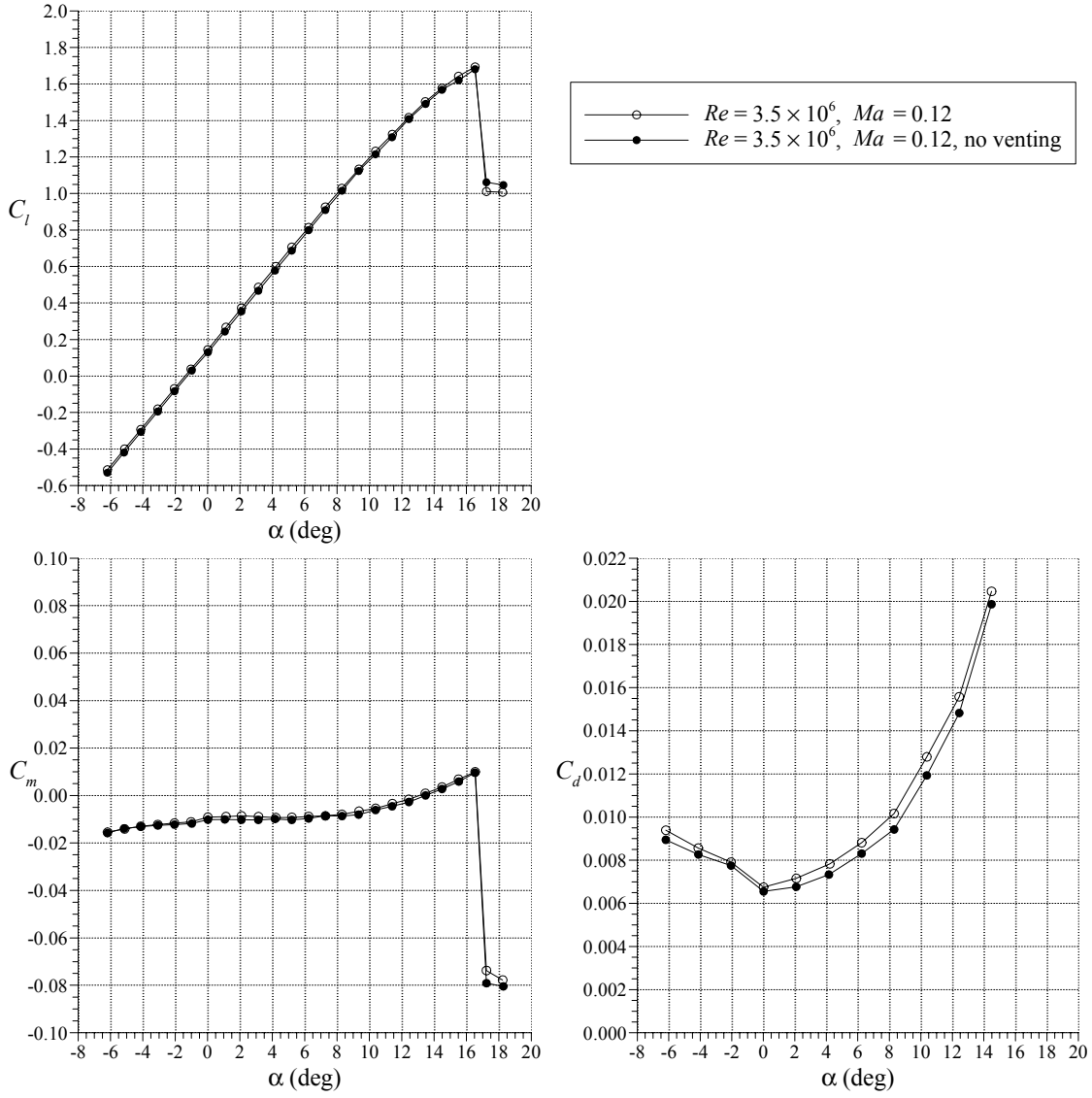

FIGURE A-1. EFFECT OF SIDEWALL VENTING ON THE PERFORMANCE OF THE CLEAN NACA 23012 AIRFOIL AT $Re = 3.5 \times 10^6$

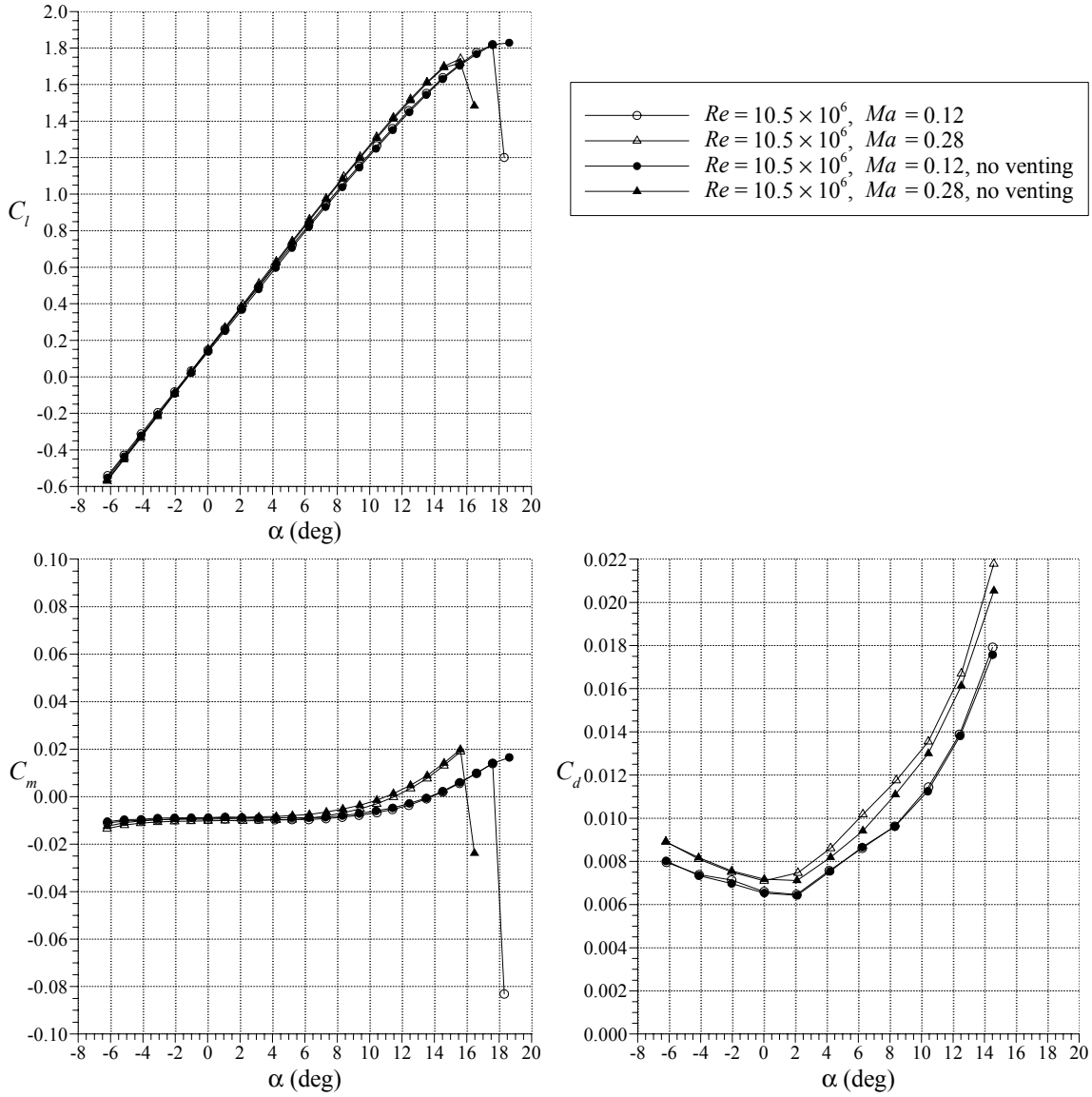

FIGURE A-2. EFFECT OF SIDEWALL VENTING ON THE PERFORMANCE OF THE CLEAN NACA 23012 AIRFOIL AT $Re = 10.5 \times 10^6$

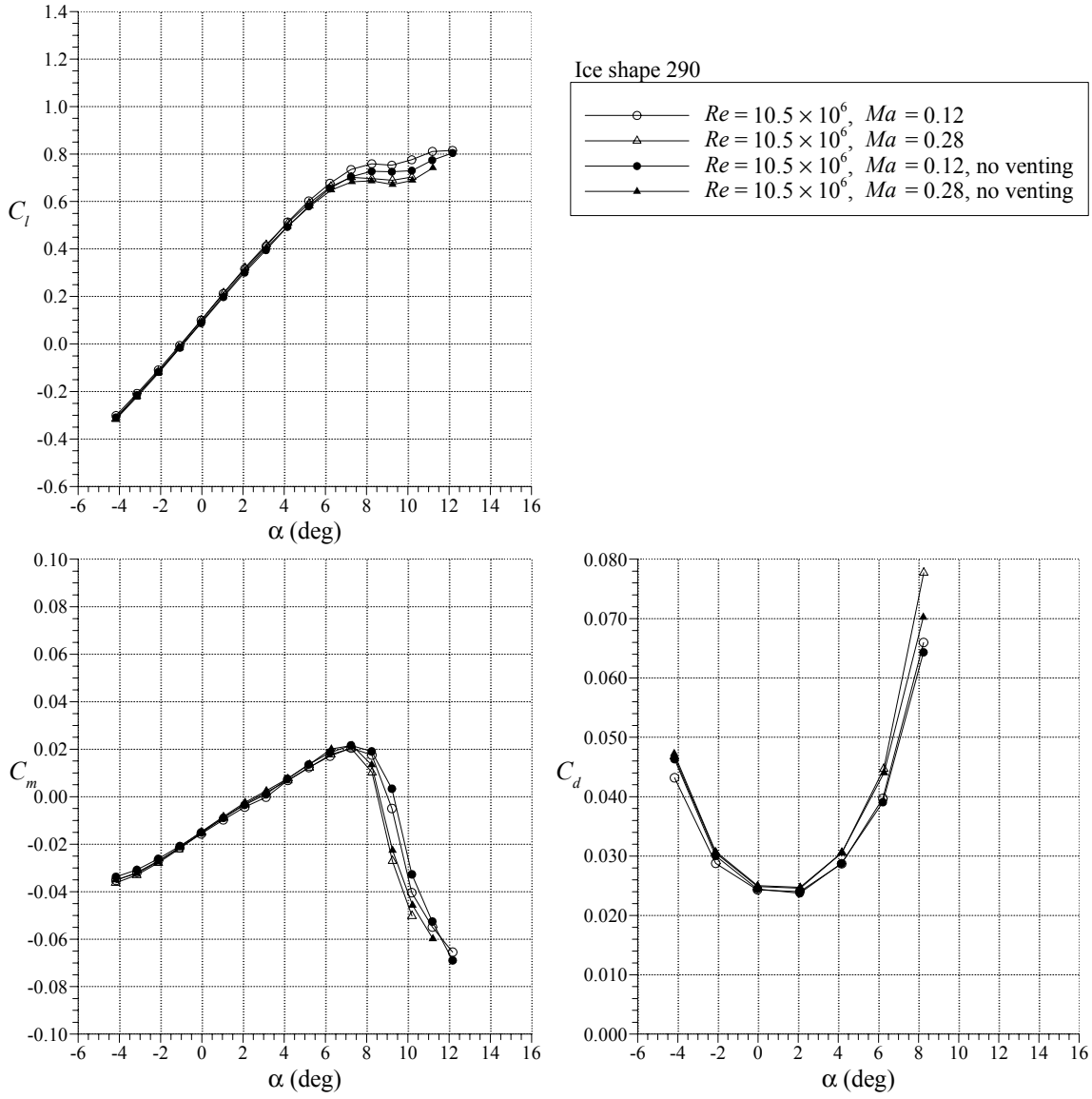

FIGURE A-3. EFFECT OF SIDEWALL VENTING ON THE PERFORMANCE OF THE NACA 23012 AIRFOIL WITH ICE SHAPE 290

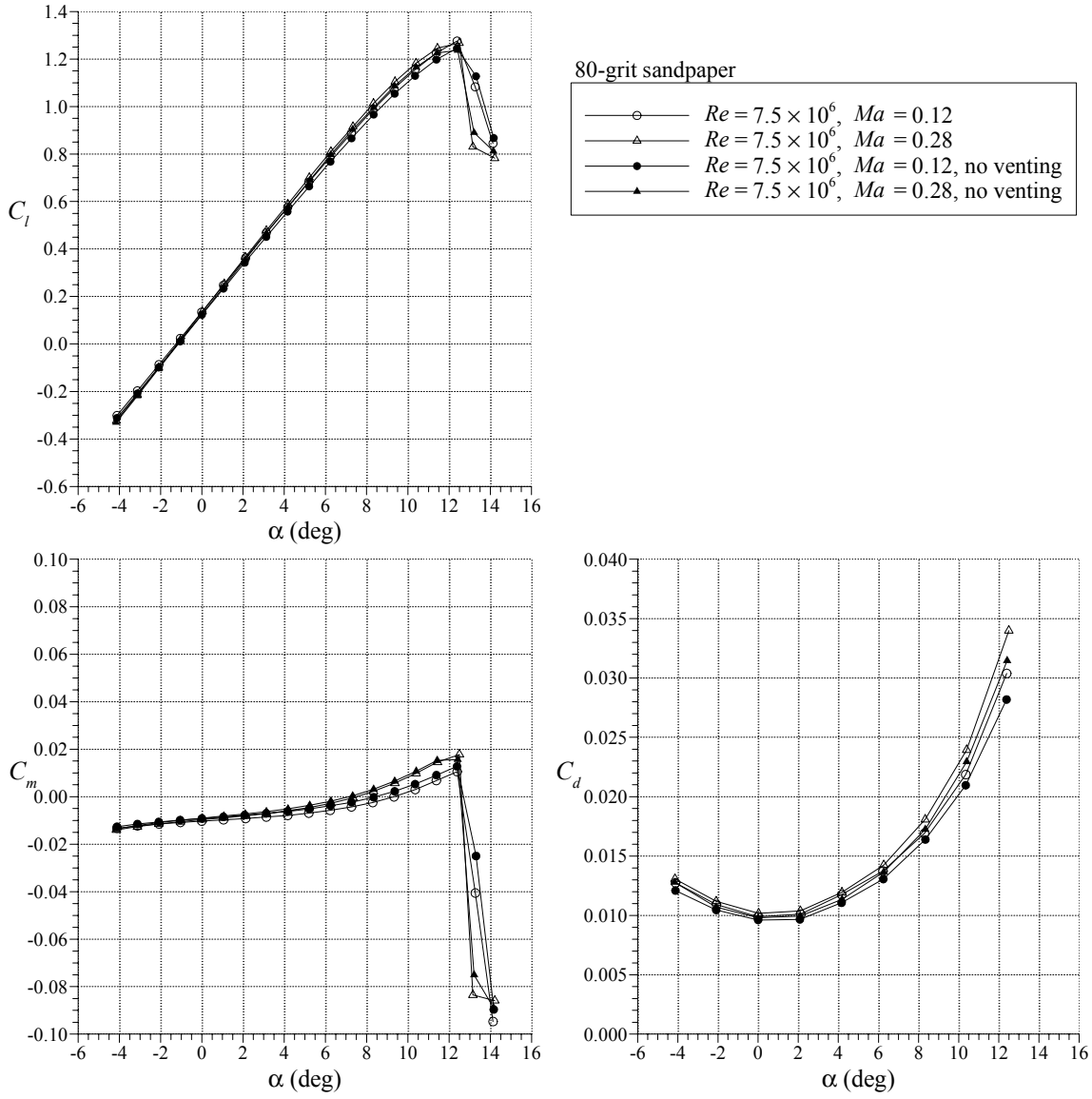

FIGURE A-4. EFFECT OF SIDEWALL VENTING ON THE PERFORMANCE OF THE NACA 23012 AIRFOIL WITH 80-GRIT SANDPAPER

APPENDIX B—FURTHER ANALYSIS OF CLEAN AIRFOIL DATA

The discussion of the clean airfoil results in section 3.3.1 included comparisons to the historical data of Abbott and von Doenhoff. These comparisons showed very good agreement for the lift coefficient variation with angle of attack, but poor agreement for the pitching moment and drag data. The purpose of this appendix is to explore this disagreement in more detail.

An additional tool was used to provide another standard for evaluation of the clean airfoil data. XFOIL[*] is an airfoil analysis code that couples a panel method flow field solver to an integral boundary-layer formulation. Several cases were run to compare with the experimental data and these results are highlighted here. Figure B-1 shows XFOIL results co-plotted with the present data and the Abbott and von Doenhoff data. The lift coefficient plot shows that the XFOIL results agree very well with the experimental data up to about 9° angle of attack. At this point and for higher angles, XFOIL over-predicts the lift coefficient. It is the authors' experience that this overprediction of lift is a common feature of XFOIL results. The pitching moment, on the other hand, has a slight offset from the present data at lower angles of attack, with the agreement being better at higher angles. The calculations also show that Abbott and von Doenhoff's pitching-moment data are not very reliable for the reasons discussed in section 3.3.1. The figure shows that the XFOIL predicted drag is more comparable to the historical data than the present data. The underprediction of minimum drag is also a common characteristic of XFOIL results in the authors' opinion. It is interesting to note, however, that the XFOIL drag crosses over and becomes higher than the Abbott and von Doenhoff drag at a C_l of approximately 1.0. This is slightly less than the C_l where the XFOIL lift data depart from the experimental results.

As noted in section 3.3.1 the drag values for the present data are consistently higher than for the historical data. This could be due to any number of factors given the differences in model and changes in the facility over the years. One factor that cannot be overlooked is that the present airfoil model was built with a removable leading edge. This was done to facilitate the attachment of the intercycle ice shape castings. However, the removable leading edge resulted in an upper and lower surface spanwise seam at x/c = 0.21. Ideally, this seam would have been smooth so as not to cause any flow disturbance. However, in practice, this was difficult to achieve and there was some discontinuity on the order of a few thousandths of an inch. It is possible that this slight discontinuity could have caused boundary-layer transition at this location.

This possibility was investigated using XFOIL. The results from the calculations (see figure B-1) showed that boundary-layer transition on the upper surface occurred downstream of x/c = 0.21 for angles of attack less than 2°. Boundary-layer transition occurred on the lower surface downstream of x/c = 0.21 for angles of attack greater than -1°. Using this information, another set of calculations was performed where the transition location was fixed at the seam (i.e., at x/c = 0.21) on the upper surface for angles of attack less than 2° and on the lower surface for angles of attack greater than -1°. These results are summarized in figure B-2. As expected, the changes in the lift and pitching moment are miniscule, whereas there is a significant increase in the airfoil drag. The XFOIL drag data with transition fixed at the leading-edge seam

[*] Drela, M., "XFOIL 6.6 User Primer," MIT Aero and Astro Engineering, March 14, 1996.

compares much more favorably with the experimental data. While this calculation is by no means conclusive, it does show that the removable leading edge (plus pressure taps, etc.) may play a role in the departure in drag values from the Abbott and von Doenhoff data. This sort of trade-off was expected, given the necessary compromises in model quality required to perform the ice shape testing.

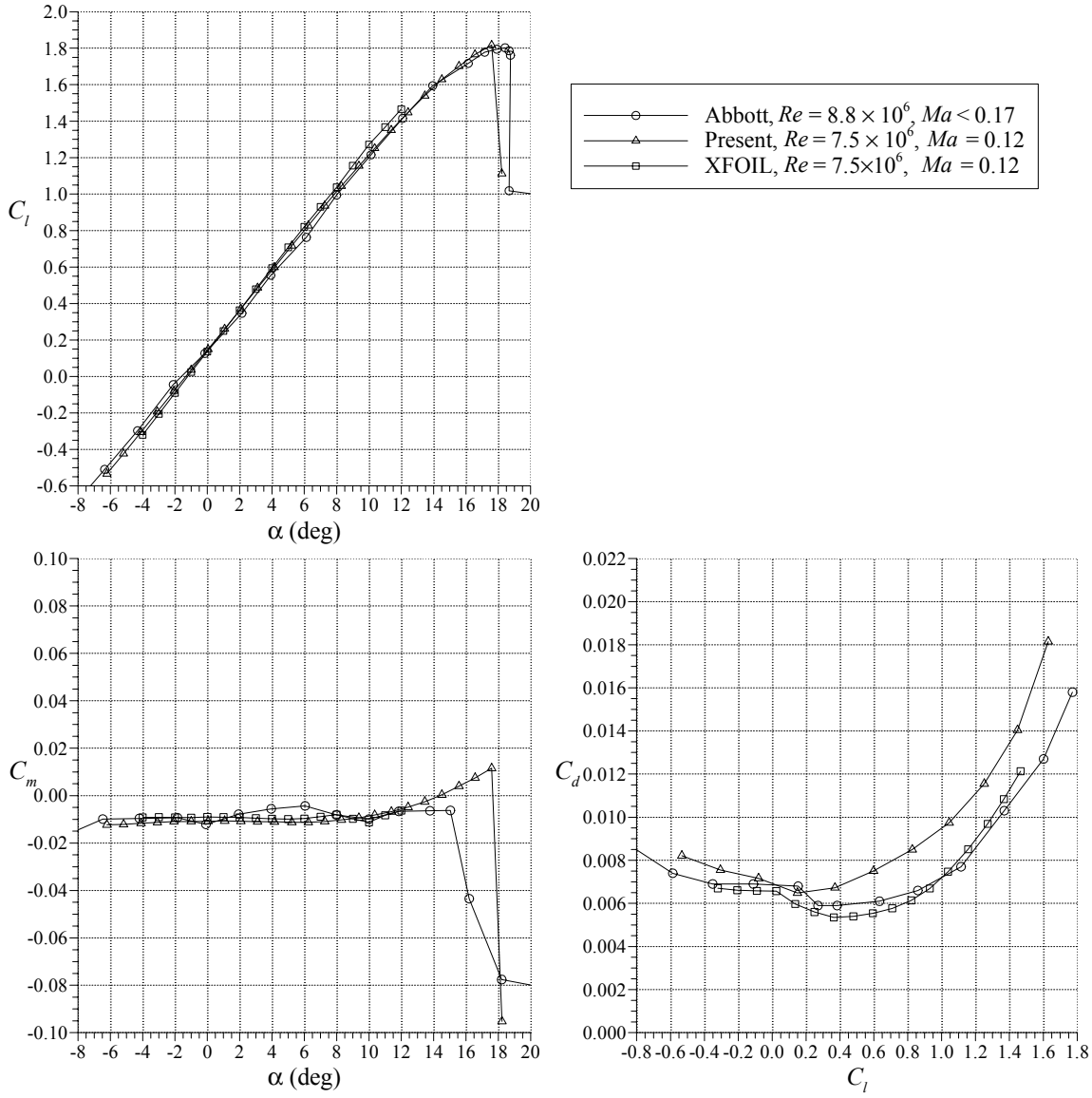

FIGURE B-1. COMPARISON OF CLEAN NACA 23012 AIRFOIL PERFORMANCE DATA WITH ABBOTT AND VON DOENHOFF DATA AND XFOIL CALCULATIONS

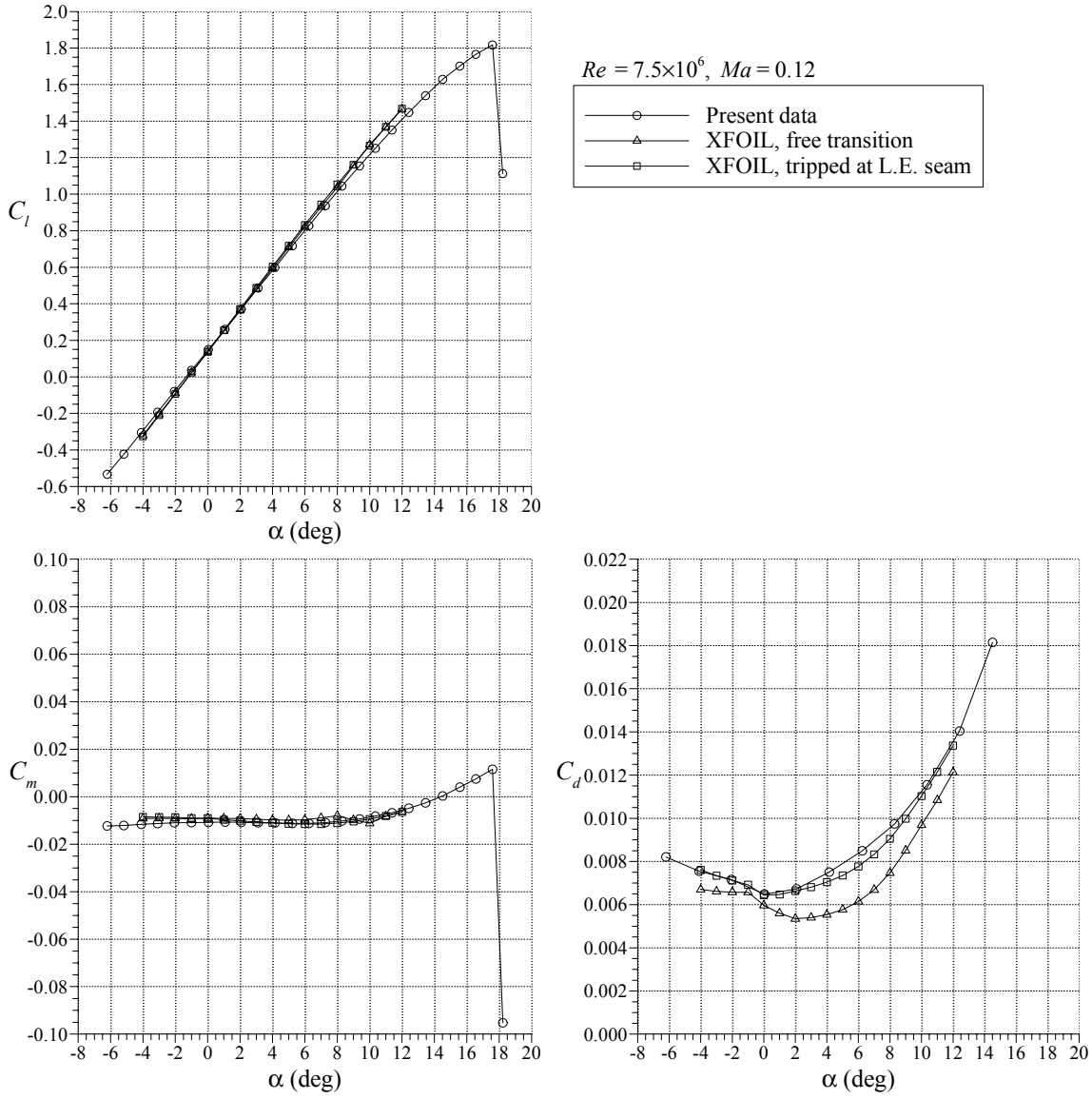

FIGURE B-2. COMPARISON OF CLEAN NACA 23012 AIRFOIL PERFORMANCE DATA WITH XFOIL CALCULATIONS FOR FREE AND FIXED TRANSITION CASES